LEVEL

DEPARTMENT OF PHYSICS

The Catholic University of America

Washington, D.C. 20064

79 03 14 020

Dynamics of Acoustic Resonance Scattering

From Spherical Targets

J. George, H. Überall, A. Farhan, G.

Mezzorani, A. Nagl and K. Sage [a]

Physics Department, The Catholic University
of America - Washington, D. C. 20064

and

J. D. Murphy
3709 Merlin Way, Annandale, VA 22003

Abstract

A resonance theory of acoustic scattering from penetrable
bodies has recently been developed (L. Flax, L. R. Dragonette,
and H. Überall, J. Acoust. Soc. Am. 63, 1690 (1978)) which
describes the features of the scattering amplitude in terms of
a background amplitude like that of an impenetrable scatterer
with superimposed resonances at the known eigenfrequencies of
the body. In the present study (carried out for the example
of a spherical gas bubble in a fluid which in spite of its
simplicity contains all the essential features of the scattering
process), the existence of these resonances is explained by the
phase-matching of surface waves on the scatter whose phase and
group velocities are obtained here. In addition, we study the
dynamics of the interior motions inside the body during the
scattering process, which are shown to undergo resonances in
the radial and angular directions except for the radial motions
on the surface, resulting in the fact that the modal surface
deformations do not exhibit any particular resonance effects at
the eigenfrequencies of the body

a) Now also at the Office of Marine Technology, Engineering
Development Laboratory, NOAA, Riverdale, MD   20840

79 03 14 020

REPORT DOCUMENTATION PAGE		READ INSTRUCTIONS BEFORE COMPLETING FORM
1. REPORT NUMBER	2. GOVT ACCESSION NO.	3. RECIPIENT'S CATALOG NUMBER
4. TITLE (and Subtitle) Dynamics of Acoustic Resonance Scattering from Spherical Targets		5. TYPE OF REPORT & PERIOD COVERED Technical Report (interim) Nov. 1, 1977-Jan. 31, 1979
		6. PERFORMING ORG. REPORT NUMBER
7. AUTHOR(s) J. George, H. Uberall, A. Farhan, G. Mezzorani, A. Nagl, K.A. Sage & J.D. Murphy		8. CONTRACT OR GRANT NUMBER(s) ONR N00014-76-C-0430
9. PERFORMING ORGANIZATION NAME AND ADDRESS Department of Physics Catholic University of America Washington, DC 20064		10. PROGRAM ELEMENT, PROJECT, TASK AREA & WORK UNIT NUMBERS Program 61153M, Project RR011-08, Task RR011-08-01 Work Unit NR 384-914
11. CONTROLLING OFFICE NAME AND ADDRESS Office of Naval Research Physics Program Office Arlington, VA 22217		12. REPORT DATE January 21, 1977
		13. NUMBER OF PAGES 40 pp + 23 pp figs. + 2 pp Form 1473
14. MONITORING AGENCY NAME & ADDRESS(If different from Controlling Office)		15. SECURITY CLASS. (of this report) Unclassified
		15a. DECLASSIFICATION/DOWNGRADING SCHEDULE

16. DISTRIBUTION STATEMENT (of this Report)

Approved for public release; distribution unlimited

17. DISTRIBUTION STATEMENT (of the abstract entered in Block 20, if different from Report)

18. SUPPLEMENTARY NOTES

19. KEY WORDS (Continue on reverse side if necessary and identify by block number)

Acoustic scattering; Resonances of Elastic Objects; Breit-Wigner Resonances; Regge Poles; Eigenvibrations of Elastic Objects; Surface Waves.

20. ABSTRACT (Continue on reverse side if necessary and identify by block number)
A resonance theory of acoustic scattering from penetrable bodies has recently been developed (L. Flax, L. R. Dragonette, and H. Uberall, J. Acoust. Soc. Am. 63, 1690 (1978)) which describes the features of the scattering amplitude in terms of a background amplitude like that of an impenetrable scatter, with superimposed resonances at the eigenfrequencies of the body. In the present study (carried out for the example of a spherical gas bubble in a fluid which in spite of its simplicity contains all the essential—

DD FORM 1473 EDITION OF 1 NOV 65 IS OBSOLETE
1 JAN 73
S/N 0102-LF-014-6601

features of the scattering process), the existence of these resonances is explained by the phase-matching of surface waves on the scatter whose phase and group velocities are obtained here. In addition, we study the dynamics of the interior motions inside the body during the scattering process, which are shown to undergo resonances in the radial and angular directions except for the radial motions of the surface, resulting in the fact that the modal surface deformations do not exhibit any particular resonance effects at the eigenfrequencies of the body.

ACCESSION for

NTIS   White Section ☑
DDC   Buff Section ☐
UNANNOUNCED   ☐
JUSTIFICATION

BY
DISTRIBUTION/AVAILABILITY CODES
     SPECIAL

A

FOREWORD

In this study, we investigate the dynamics of surface motion of a penetrable spherical body subjected to an incident place acoustic wave. The results should be valid for objects of rather general internal consistency since they are based on quite basic physical considerations, but they are illustrated here by the example of a gas bubble in a fluid. It is shown that surface waves generated in the scattering process circumnavigate the target sphere and, by a process of in-phase "resonance reinforcement", excite its multipole resonances at those eigenfrequencies at which n + 1/2 wavelenghts (n being are integer) span the circumference. Phase matching is achieved here due to the fact that the surface wave suffers a phase jump of $\pi/2$ at each of the two "caustic points" on the sphere at which the surface waves converge. Surface motions and circumferential waves on the bubble are graphically demonstrated, both on and off resonance. It is shown that the resonance manifests itself by a large-amplitude angular oscillation of the gas contained in the bubble.

Introduction

Recently, some progress in dynamical studies of sound scattering from elastic objects[1] was achieved by linking the excitation of resonances of the target body during the scattering process to a resonant reinforcement of diffracted "creeping waves" in their multiple circumnavigations of the body. In this way, the occurence of acoustic scattering resonances, and more fundamentally, the very existence of the eigenvibrations of an elastic body, has been traced back to a dynamic origin rooted in the phenomenon of circumferential waves that exist on the surface of the body, and partly also in the ambient medium. Corresponding resonances appear in the surface waves themselves[2], and, as shown by Flax, Dragonette and Überall[3] who following a suggestion of L. Flax used the methods of nuclear scattering theory for this purpose, these resonances become manifest also in the individual partial waves of a normal mode expansion of the field where they interfere with a smooth "potential scattering" background characteristic of an impenetrable (rigid, soft[3,4], or intermediate[5]) target object. Similar results were also observed to hold in the scattering of elastic waves from cavities[6-10].

The link between creeping waves and eigenvibrations for a spherical target takes a somewhat different, and more interesting, form than for the cylindrical bodies discussed earlier[1-3,10]. The eigenvibrations and related creeping waves of spherical bodies will thus be discussed in the following, considering the special case of gas-filled bubbles in a fluid medium. Although this example constitutes the simplest kind of scattering problem, it exhibits all the basic features of the creeping-wave resonances to be discussed here; and it represents an interesting problem in its own right, for which prior to our recent discussion[11], only scant knowledge existed[12] concerning all the higher multipole resonances (apart from the well-known[13] fundamental "breathing-mode" monopole resonance, of course).

It will be shown below that the sound scattering phenomenon with a spherical target bubble can be resolved into the creation of a manifold of circumferential waves (represented by "Regge poles" in the scattering amplitude), which circumnavigate the target with various phase velocities that depend on the frequency. Their dispersion curves (as well as their trajectories in the complex mode number plane) may be obtained from the calculated progression of the modal resonances to higher frequencies with increasing mode number, as studied by us earlier[11]. These resonances were shown

there to be superimposed on, and to interfere with, a smooth background amplitude corresponding to the scattering from a pressure-release sphere, for the case of an air bubble in water. We now demonstrate that resonance takes place in the nth mode at any such frequency at which one of the circumferential waves spans the circumference of the bubble $n + \frac{1}{2}$ times, n being an integer. It is shown in addition that all these creeping waves converge at the vertex and at its antipode on the sphere, and lose a quarter-wavelength (corresponding to a phase jump of $\pi/2$) upon passage through each one of these two caustic points. One full circumnavigation thus leads to perfect phase matching when the above condition of $n + \frac{1}{2}$ geometrical wavelengths equalling the circumference is satisfied, and hence to a resonant reinforcement of the creeping wave during its repeated circumnavigations. This phenomenon forms the basis for the resonant eigenvibrations of a gas bubble in a fluid, an explanation which will also hold for target bodies of more general (e.g. elastic, layered, etc.) consistency and for the excitation of their eigenvibrations by more general, non-acoustic forces. The very existence of the eigenvibrations of elastic objects may then, in a sense, be referred back to the existence of circumferential waves on their surface, and to the resonant reinforcements of the latter in the course of their repeated circumnavigations.

We have carried out numerical calculations in order to demonstrate the phase matching of the surface waves. Further numerical calculations were done for study of the displacement of the air particles in the bubble on and off the resonance. It is found that at resonance, the air motion in the bubble is enhanced by a factor $\sim 10^3$, except for the radial component of motion on the bubble surface. This results in the fact that the modal bubble surface deformations do not exhibit any particular resonance effects at the eigenfrequencies of the bubble.

I. Modal Resonances of a Gas Bubble in a Fluid

The scattering of sound by a fluid (or gaseous) sphere imbedded in another fluid may be discussed in terms of a velocity potential $\phi(\vec{r})$, from which the particle velocity field $\vec{v}$ is obtained via

$$\vec{v} = -\vec{\nabla}\phi. \tag{1}$$

The total (incident plus scattered) field is given[11] by the normal-mode series

$$\phi = \phi_0 \, e^{-i\omega t} \sum_{n=0}^{\infty} (2n+1) \, i^n \left[j_n(kr) + A_n \, h_n^{(1)}(kr) \right] P_n(\cos\vartheta) \tag{2}$$

where j_n is due to the incident and $h_n^{(1)}$ to the scattered wave. Here, ϕ_0 is the amplitude of the incident plane wave, and $k = \omega/c$ its wave number is the ambient fluid. Satisfying the boundary conditions (continuity of pressure and of normal particle velocity) at the spherical surface $r = a$ determines the scattering coefficient A_n of the nth mode as

$$A_n = -\, \frac{\rho_b \, x \, j_n(x_b) \, j_n'(x) - \rho_w \, x_b \, j_n'(x_b) \, j_n(x)}{\rho_b \, x \, j_n(x_b) \, h_n^{(1)\prime}(x) - \rho_w \, x_b \, j_n'(x_b) \, h_n^{(1)}(x)} \,, \tag{3}$$

where $x = ka$, $x_b = k_b a$ with $k_b = \omega/c_b$ being the wave number of sound inside the bubble; ρ_b and ρ_w are the fluid density inside and outside the bubble, respectively.

Following our previous study, we rewrite Eq. (3) in the form

$$A_n = \frac{S_n^{(0)}}{2} \frac{z_n^{(2)} - z_n^{(1)}}{z_n^{(1)} - F_n} + \frac{1}{2}\left(S_n^{(0)} - 1\right) \tag{4}$$

where

$$S_n^{(0)} = -h_n^{(2)}(x)/h_n^{(1)}(x) \equiv e^{2i\xi_n}, \tag{5a}$$

$$z_n^{(i)} = x\, h_n^{(i)\prime}(x)/h_n^{(i)}(x), \qquad i = 1,2 \tag{5b}$$

$$F_n = (\rho_w/\rho_b)\, x_b\, j_n'(x_b)/j_n(x_b). \tag{5c}$$

The last term in Eq. (4) corresponds to the scattering coefficient for the limit of a pressure-release sphere, where $\rho_b/\rho_w \to 0$ and $F_n \to \infty$. Reference 11 further showed that after a Taylor expansion, Eq. (4) becomes approximately

$$A_n \cong e^{2i\xi_n}\left[\sum_{\ell=0}^{\infty} \frac{-(i/2)\Gamma_{n\ell}}{x - x_{n\ell} + (i/2)\Gamma_{n\ell}} + i\, e^{-i\xi_n} \sin\xi_n\right] \tag{6}$$

where $x_{n\ell}$ is the ℓth resonance frequency of the bubble contained in the nth normal mode of the scattering amplitude as determined from the eigenvalue equation

$$\text{Re } z_n^{(1)} = F_n. \tag{7}$$

The resonance width $\Gamma_{n\ell}$ is given by

$$\Gamma_{n\ell} = (2/\beta_{n\ell}) \, Im \, z_n^{(1)},$$

(8a)

where

$$\beta_{n\ell} = (d/dx) \left[Re \, z_n^{(1)} - F_n \right]_{x=x_{n\ell}}.$$

(8b)

Eq. (6) indicates that the amplitude consists of a smooth background due to scattering from a pressure release sphere (second term), super-imposed upon which there is a series of interfering resonances (first term). This is demonstrated in Fig. 1 where we plot the quantities $|f_n(\vartheta)|$ for $\vartheta = \pi$ $(n \leqslant 3)$ vs. $x \equiv ka$ up to $x = 4$ for an air bubble in water, where

$$f_n(\vartheta) = (1/k)(2n+1) A_n P_n(\cos\vartheta)$$

(9)

is the asymptotic scattering amplitude ("form function"). The smooth background is clearly visible, and the interfering resonance peaks are labeled by (n, ℓ). The tall resonance peak $(0,1)$ represents the well-known[13] giant monopole bubble resonance. The resonance frequencies, obtained from a numerical solution of Eq. (7), are also given in Table I up to $x \leqslant 4$.

II. Circumferential Waves and Their Resonances

In the nuclear scattering theory formalism[14], one usually rewrites Eq. (2) as $\phi = \phi_{in} + \phi_{out}$, where the amplitude of spherically outgoing waves is

$$\phi_{out} = \frac{\phi_0}{2} e^{-i\omega t} \sum_{n=0}^{\infty} (2n+1) i^n S_n h_n^{(1)}(kr) P_n (\cos \vartheta),$$ (10)

with the "scattering function"

$$S_n = 2A_n + 1 .$$ (11)

Due to Eq. (6), S_n has poles in the lower half of the complex x-plane, located at

$$x = x_{n\ell} - (i/2) \Gamma_{n\ell} .$$ (12)

These may, however, be rewritten in the form of poles in the complex n-plane, by treating n as a continuous variable and expanding

$$x_{n\ell} \cong x_{n_\ell \ell} + (n - n_\ell) x'_{n_\ell \ell} + \cdots$$ (13)

($x'_{n_\ell \ell} > 0$, see Fig. 1, where $x'_{n\ell} = (d/dn) x_{n\ell}$), about an n-value n_ℓ chosen so that $x_{n_\ell \ell} = x$ (the given incident frequency). The S-function, which reads

$$S_n \equiv S_n^{(0)} \frac{z_n^{(2)} - F_n}{z_n^{(1)} - F_n} \cong S_n^{(0)} \sum_{\ell=0}^{\infty} \frac{x - x_{n\ell} - (i/2) \Gamma_{n\ell}}{x - x_{n\ell} + (i/2) \Gamma_{n\ell}}$$ (14)

(note that the various terms in the sum are accurate only in the immediate vicinity of their resonance peaks), can then be rewritten in the form

$$S_n \cong S_n^{(0)} \sum_{\ell=0}^{\infty} \frac{n - n_\ell + (i/2)\hat{\Gamma}_{n_\ell \ell}}{n - n_\ell - (i/2)\hat{\Gamma}_{n_\ell \ell}} \equiv S_n^{(0)} \sum_{\ell=0}^{\infty} \frac{n - \hat{n}_\ell^*}{n - \hat{n}_\ell} \qquad (15a)$$

where

$$\hat{\Gamma}_{n_\ell \ell} = \Gamma_{n_\ell \ell} / X'_{n_\ell \ell} , \qquad (15b)$$

indicating the existence of "Regge poles"[14] in the scattering function located at the positions $\hat{n}_\ell$, where

$$\hat{n}_\ell = n_\ell + (i/2) \hat{\Gamma}_{n_\ell \ell} , \qquad (15c)$$

in the upper half of the complex n-plane.

These Regge poles, and their residues, are conventionally obtained by performing a Watson transformation on Eq. (10), whereby a series of the form $\sum \mathcal{G}_n P_n$ is rewritten[14] as a contour integral:

$$\sum_{n=0}^{\infty} \mathcal{G}_n P_n (\cos \vartheta) = -(i/2) \oint_C \mathcal{G}_{\nu - \frac{1}{2}} \frac{P_{\nu - \frac{1}{2}} (-\cos \vartheta)}{\cos \pi \nu} d\nu , \qquad (16a)$$

C being a clockwise contour enclosing the positive real axis in the complex ν plane. Applying this to Eq. (10) with an appropriate expression for $\mathcal{G}_n$, one may then re-evaluate the contour integral

at the Regge poles $\nu = \hat{n}_\ell + \frac{1}{2}$ of the function $\mathcal{Y}_{\nu - \frac{1}{2}}$, written in the form

$$\mathcal{Y}_{\nu - \frac{1}{2}} = \sum_{\ell=0}^{\infty} \frac{\mathcal{Y}_{\nu - \frac{1}{2}}^{(\ell)}}{\nu - \frac{1}{2} - \hat{n}_\ell} \tag{16b}$$

in order to exhibit the denominator in Eq. (15a). This leads to the exact expression

$$\phi_{out} = \sum_{\ell=0}^{\infty} \mathcal{Y}_{\hat{n}_\ell}^{(\ell)} \frac{\pi \, P_{\hat{n}_\ell}(-\cos\vartheta)}{\cos\pi(\hat{n}_\ell + \frac{1}{2})}, \tag{17a}$$

with

$$\mathcal{Y}_{\hat{n}_\ell}^{(\ell)} = i\phi_0 \, e^{-i\omega t} (\hat{n}_\ell + \frac{1}{2}) e^{i\pi\hat{n}_\ell} h_{\hat{n}_\ell}^{(1)}(kr) \hat{\Gamma}_{\eta\ell} S_{\hat{n}_\ell}^{(0)} \tag{17b}$$

for the scattered wave of Eq. (10), which has the same poles and residues in the variable $\hat{n}_\ell$ at all the integers n as does Eq. (10) with the approximate expression of Eq. (15a), and we see that our consideration of the Watson transformation has furnished generalized resonance denominators which interpolate between the resonance positions, and which will be seen to provide us with a physical picture of the very origin of the resonances.

Such a picture may be obtained by using the asymptotic form[14] (valid for $\nu \sin\vartheta \gg 1$),

$$P_\nu(-\cos\vartheta) \cong \left(\frac{2}{\pi(\nu + \frac{1}{2})\sin\vartheta} \right)^{1/2} \cos\left[(\nu + \frac{1}{2})(\pi - \vartheta) - \frac{1}{4}\pi \right] \tag{18a}$$

in Eq. (17); even for small values of n, this should provide an approximate description of the general behavior of the amplitude. One may then split the cosine in Eq. (18a) into two exponentials, and expand the denominator of Eq. (17),

$$1/\cos\pi(\hat{n}_\ell + \tfrac{1}{2}) \equiv -1/\sin\pi\hat{n}_\ell = 2i\sum_{m=0}^{\infty} e^{i\pi(2m+1)\hat{n}_\ell} \quad , \tag{18b}$$

so that

$$\phi_{out} \cong i\pi\sum_{\ell=0}^{\infty}\left(\frac{2}{\pi(\hat{n}_\ell + \tfrac{1}{2})\sin\vartheta}\right)^{1/2}\varphi_{\hat{n}_\ell}^{(\ell)}\sum_{\mathcal{E}=\pm 1}\sum_{m=0}^{\infty} e^{-i\mathcal{E}\pi/4 - im\pi}e^{i(\hat{n}_\ell + \tfrac{1}{2})[\mathcal{E}(\pi - \vartheta) + 2m\pi]} \quad . \tag{19}$$

With the time factor $\exp(i\omega t)$ of Eq. (10), this shows that for $m = 0$ and a given value of ℓ, two surface waves with angular propagation constant $\hat{n}_\ell + \tfrac{1}{2}$ propagate in the counterclockwise ($\mathcal{E} = -1$) and in the clockwise ($\mathcal{E} = +1$) direction around a meridian of the bubble, with an amplitude spreading factor $\sin^{-\frac{1}{2}}\vartheta$ that describes their convergence at the north and south poles (i.e. the vertex of the sphere as seen by the incident wave, and its antipode). These "tidal waves" are joined by other such waves with $m > 0$ that already have encircled the bubble m times previously (of course with larger and larger attenuation, which is furnished by Im $\hat{n}_\ell \neq 0$), corresponding to steady-state scattering. The wavelength of these surface waves is obtained as

$$\lambda_\ell(x) = 2\pi a / \text{Re}(\hat{n}_\ell + \tfrac{1}{2}) \tag{20a}$$

$$= 2\pi a / (n_\ell + \tfrac{1}{2}) \tag{20b}$$

if Eq. (15c) is used, with n_ℓ determined by the equation $X_{n_\ell \ell} = X$. Due to radiation damping, these waves decay as $\exp(-\vartheta/\vartheta_\ell)$, where the decay angle ϑ_ℓ is found as

$$\vartheta_\ell (x) = 1 / \operatorname{Im} \hat{n}_\ell \tag{21a}$$

$$= 2 x'_{n_\ell \ell} / \Gamma_{n_\ell \ell} \tag{21b}$$

if Eq. (15c) is used, with $\Gamma_{n_\ell \ell}$ and $x'_{n_\ell \ell}$ given by Eqs. (8a) and after Eq. (13), respectively. Such surface waves have been termed "creeping waves" by Franz[15], although their discussion goes back to van der Pol[16] and before.

The phase velocity of the ℓth surface wave is seen from Eq. (19) to be

$$c_\ell (x) = \frac{a\omega}{\operatorname{Re}(\hat{n}_\ell + \frac{1}{2})} = \frac{x}{n_\ell + \frac{1}{2}} c \; ; \tag{22}$$

dispersion curves for the surface waves based on this expression will be shown below.

Using the above picture of circumnavigating surface waves excited in the scattering process, one arrives at a physical explanation for the origin of the resonances themselves. Equations (20) show that at a physical resonance ($\operatorname{Re} \hat{n}_\ell$ = integer = n, cf., e.g., Eq. (15a)), the wavelength of the surface wave is given by

$$\lambda_\ell = 2\pi a / (n + \tfrac{1}{2}). \tag{23}$$

The resonance condition, Re $\hat{n}_\ell (x) = n$, is therefore tantamount to the requirement that the bubble circumference measure an odd number of half-wavelengths of the surface wave, which may also be considered the eigenvalue equation for the resonance frequency $x_{n\ell}$. A resonance condition of this kind has already been noted by Junger and Feit[17]. Equation (23) actually leads to phase matching of the surface wave after each additional curcumnavigation, in spite of the fact that a half-integer number of wavelengths fit around the bubble circumference. This becomes clear from inspection of Eq. (19), which reveals that owing to the factors $\exp(-i\varepsilon\pi/4)$, a phase jump corresponding to $\exp(-i\pi/2)$ takes place every time the surface wave passes through the convergence zones at the north and south pole of the spherical bubble ($\vartheta = 0, \pi$). During such a passage, the continuing description of a surface wave encircling the bubble in a given sense passes[18] from one exponential in Eq. (19) to the other one, the relative difference in the factors $\exp(-i\varepsilon\pi/4)$ providing the mentioned phase jump. Since the latter amounts to a backward shift of the wave by an extra $\frac{1}{4} + \frac{1}{4}$ wavelengths (at each pole) = $\frac{1}{2}$ wavelength during one complete circumnavigation, the condition $2\pi a = (n + \frac{1}{2})\lambda$ actually results in

an exact phase matching of the surface wave with itself after each complete circuit, which explains physically the appearance of a resonance as a resonant reinforcement of the tidal waves in the course of their repeated circumnavigations. If unattenuated, such a reinforcement would cause infinite amplitudes. The radiative attenuation of the surface wave leads to finite amplitudes and a finite resonance width.

As mentioned, the north and south pole represent caustic points for the surface waves on the bubble. A corresponding phase jump of $\pi/4$ for a wave passing through a caustic is well-known for other examples in acoustics, e.g. sound propagation through the inhomogeneous oceanic medium[19].

The phase matching condition may be viewed somewhat differently, namely as a coincidence condition for phase velocities. The vibrational modes continued in Eq. (10), being standing circumferential waves around the bubble circumference, may each be decomposed into a pair of modal waves propagating in opposite directions with phase velocities c_ℓ, using the separation[20]

$$P_v(-\cos\vartheta) = \tfrac{1}{2}\left[P_v(-\cos\vartheta) - \tfrac{2i}{\pi}Q_v(-\cos\vartheta)\right] + \tfrac{1}{2}\left[P_v(-\cos\vartheta) + \tfrac{2i}{\pi}Q_v(-\cos\vartheta)\right]$$

$$\cong \left[2/\pi(v+\tfrac{1}{2})\sin\vartheta\right]^{1/2}\left\{\tfrac{1}{2}e^{i\left[(v+\tfrac{1}{2})(\pi-\vartheta)-\pi/4\right]} + \tfrac{1}{2}e^{-i\left[(v+\tfrac{1}{2})(\pi-\vartheta)-\pi/4\right]}\right\} \tag{24}$$

as shown in Fig. 2 for the quadrupole (n = 2). The acoustic scattering process generates a series of surface waves with speeds $c_\ell(x)$ around

the bubble given by Eq. (22), while using Eqs. (10) and (18), the modal speeds are given by

$$\mathcal{C}_n = a \omega / (n + \tfrac{1}{2}).$$

(25)

From Eq. (22), it is seen that a resonance occurs at that frequency $x_{n\ell}$ at which the speed of the ℓth surface wave launched during the scattering process coincides with the phase velocity of the modal wave corresponding to the nth natural multipole vibrational mode of the bubble. Again, this coincidence condition for phase velocities may be viewed as an eigenvalue condition for $x_{n\ell}$.

III. Numerical Results

In the following, we shall obtain some numerical results of the properties of surface waves as they are excited by plane acoustic waves incident on an air bubble in water.

1.) Phase and group velocities.

The phase velocity of the ℓth surface wave is given by Eq. (22). In Fig. 3a, we plot the ratios c_ℓ /c as a function of $x \equiv ka$ for $\ell = 1$ through 14. The ensuing dispersion curves, which are not unlike those for the Lamb waves or a fluid layer in a vacuum[21], come in from infinity at some low-frequency cutoff (except for the $\ell = 0$ wave), and at high

frequencies they all appear to approach the common value $c_b/c = 0.22$, where c_b is the sound velocity in the fluid contained in the bubble (here, air).

If we introduce a trace velocity $c_{tr} = c/\sin \alpha$ of the incident plane wave on the surface of the sphere, where α is the angle of the surface normal with the direction of incidence, then Cremer's "coincidence condition"[22] $c_{tr} = c_\ell$ between the incident-wave trace velocity and the surface wave speed determines the angle α at which the surface wave is launched. The infinite values of c_ℓ at the cutoffs in Fig. 3a thus correspond to a launching angle $\alpha = 0$. At those frequencies where $c_\ell \leq c$, the launching presumably then occurs at lancing incidence, $\alpha = 90°$, if an excitation of these waves does take place at all.

The group velocity of the ℓth surface wave is given by[1]

$$c_\ell^{gp}(x) = \frac{a}{d \, Re \, (\tilde{n}_\ell + \frac{1}{2})/d\omega} = \frac{dx}{dn_\ell} c.$$

(26)

In Fig 3b, we plot the ratios c_ℓ^{gp}/c as a function of $x \equiv ka$ for $\ell = 1$ through 14. They were obtained from our calculated resonance frequencies which only covered a limited region, so that some portions of the graph remained open.

2.) Circumferential Waves

We shall here illustrate the propagation of the previously

discussed circumferential waves around the bubble during the scattering process, exhibiting the $-\pi/2$ phase jump at the poles of the sphere and the phase matching at resonance. Note that the field ϕ_{out} of Eq. (19) actually describes the **total** field ϕ ($= \phi_{in} + \phi_{out}$) outside the bubble, since ϕ_{in} does not contain the S function with its Regge poles, hence furnishes no contribution in the residue evaluation of the Watson integral.

After expanding the denominator of Eq. (17a) as in Eq. (18b), we obtain using Eq. (24):

$$\phi = \sum_{\ell, m = 0}^{\infty} I_+ \, (\beta, \ell, m) + \sum_{\ell, m = 0}^{\infty} I_- (\beta, \ell, m) \tag{27a}$$

with

$$I_{\pm} \, (\beta, \ell, m) = \pi i \, \oint_{\hat{n}_\ell} \varphi^{(\ell)} e^{(2m+1)\pi i \hat{n}_\ell} \left[P_{\hat{n}_\ell} (-\cos\vartheta) \mp \frac{2i}{\pi} Q_{\hat{n}_\ell} (-\cos\vartheta) \right] \tag{27b}$$

or, asymptotically:

$$I_{\pm} \, (\beta, \ell, m) \cong \pi i \left(\frac{2}{\pi (\hat{n}_\ell + \frac{1}{2}) \sin\vartheta} \right)^{1/2} \varphi_{\hat{n}_\ell}^{(\ell)} \, e^{(2m+1)\pi i \hat{n}_\ell} \, e^{\pm i \left[(\hat{n}_\ell + \frac{1}{2}) \alpha - \frac{\pi}{4} \right]} \tag{27c}$$

where $\alpha = \pi - \vartheta$, and $\beta = 2 m \pi \pm \alpha$ is the continuosly increasing phase angle around the sphere, cf. footnote 18. For a given label ℓ characterizing the order of the surface wave, this describes two waves encircling the bubble

in opposite directions with angular propagation constant

$\hat{n}_\ell + \frac{1}{2}$. We shall represent graphically one of these

waves by the surface deformation which it causes. The

deformation is determined by the deformed radius,

$$R_\pm^{(\ell)}(a,\vartheta) = a + \text{Re } u_r^{(\ell)\pm}(a,\vartheta), \tag{28a}$$

and the radial displacement is given exactly by

$$\text{Re } u_r^{(\ell)\pm}(a,\vartheta) = \sum_{m=0}^{\infty} \left(\frac{\pi}{2}\right)^{1/2} \Phi_0 \left(n_\ell + \frac{1}{2}\right) \left| h_{n_\ell}^{(1)\,\prime}(x) \right| \tag{28b}$$

$$\cdot \text{Re} \left\{ e^{(2m+1)\pi i\, n_\ell} \left[P_{n_\ell}(-\cos\vartheta) \mp \frac{2i}{\pi} Q_{n_\ell}(-\cos\vartheta) \right] \right\},$$

or asymptotically (for $n_\ell \sin\vartheta \gg 1$) by

$$\text{Re } u_r^{(\ell)\pm}(a,\vartheta) \cong \sum_{m=0}^{\infty} \Phi_0 \left(n_\ell + \frac{1}{2}\right)^{1/2} \left| h_{n_\ell}^{(1)\,\prime}(x) \right| (\sin\vartheta)^{-1/2} \tag{28c}$$

$$\cdot \cos\left\{ \pm \left(n_\ell + \frac{1}{2}\right)\left[\alpha \pm (2m+1)\pi\right] - (2m+1)\frac{\pi}{2} \mp \frac{\pi}{4} \right\},$$

with an amplitude factor

$$\Phi_0 = \left[(2\pi)^{1/2}/c \right] \phi_0 \, \hat{\Gamma}_{n_\ell \ell} \, , \tag{28d}$$

where due to the narrowness of the resonances (Fig. 1) and

the ensuing weak attenuation, we were able to approximate

$\hat{n}_\ell \cong n_\ell$ for the case of the air bubble in water.

In Fig. 4 and 5, we plot the amplitude of the surface

deformation caused by circumferential waves as given by Eq.

(28 a), for various cases on and off resonance. The plots

are done on an arbitrary scale, only the wave which

progresses in the clockwise sense is shown, and $\left| h_{n_\ell}^{(1)\prime}(x) \right|$

is approximated by a constant in the vicinity of each

resonance. In addition, we multiply the displacement

amplitude $\mathrm{Reu}_r^{(\ell)}$ by $(\sin\vartheta)^{\frac{1}{2}}$ in order to remove the

corresponding singularity which is merely caused by the

geometrical convergence of the waves at the poles of the

sphere.

Fig. 4a shows a surface wave with $n_\ell = 4.7$, so that we

are close to the resonance case $n_\ell = 5$ at which 5.5 wave-

lengths span a meridian of the sphere. It is evident that

at each of the poles at $\vartheta = 0°$ and $180°$ a phase jump

by a quarter wavelength takes place, and also that after one

circumnavigation the wave does not close into itself, so that

no resonant buildup of the amplitude will result. The solid

curve has been obtained using the asymptotic form Eq. (28c)

which is quite adequate for this value of n_ℓ , and the

dashed curve (shown here only in the vicinity of $\vartheta = 180°$)

was obtained from the exact Eq. (28 d) in which P_{n_ℓ} and

Q_{n_ℓ} with non-integer index were calculated numerically

in terms of hypergeometric series.[22] It is seen that in the

exact calculation, the phase jump is not abrupt but takes

place in a smooth fashion.

In Fig. 4b, the same quantities are plotted for $n_\ell = 5.0$, so that the surface wave closes into itself and a resonance results. We see that at $\vartheta = 180°$, the exact displacement vanishes; this takes place in such a fashion that if the geometrical amplitude factor $(\sin \vartheta)^{-\frac{1}{2}}$ is retained, the resonating amplitude remains finite at $\vartheta = 180°$. This is shown by the light dashed line on the extreme right of the figure, while the light solid line represents the asymptotic calculation, in which the factor $(\sin \vartheta)^{-\frac{1}{2}}$ causes the geometrical divergence of the amplitude which is evident here.

Analogous results are shown in Fig. 5 near and at the $n_\ell = 1$ resonance where 1.5 wavelengths fit over the meridian of the sphere. Fig. 5a shows the surface wave below the resonance, at $n_\ell = 0.7$, and Fig. 5b at the resonance, $n_\ell = 1.0$. Again the solid line results from the asymptotic and the dashed line from the exact calculation.

3.) Displacements of bubble surface and interior fluid

The particle displacement in the sound field is related to the velocity field $\vec{v}$ by $\dot{\vec{u}} = \vec{v}$, so that

$$\vec{u} = (i/\omega)\vec{v} = (i\omega)^{-1}\vec{\nabla}\phi , \qquad (29)$$

see Eq. (1). The change of shape of the bubble surface is governed by the radial displacement u_r, which is continuous

across the surface. (The angular displacement u_{ϑ} , to first order, only moves the air particles along the surface without shape change. It is discontinuos across the surface, since the air can slip relative to the water particles).

Using the scalar potential within the bubble,[11]

$$\phi_b = \phi_o \, e^{-i\omega t} \sum_{n=0}^{\infty} (2n+1) \, i^n \, B_n \, j_n(k_b r) \, P_n(\cos\vartheta), \qquad (30a)$$

where

$$B_n = (i\rho_w / x)\left[\rho_b \, x \, h_n^{(1)'}(x) \, j_n(x_b) - \rho_w \, x_b \, j_n'(x_b) \, h_n^{(1)}(x)\right]^{-1}, \qquad (30b)$$

we find for the displaced radius R_n of the bubble in its extreme positions, if only the nth mode is excited:

$$R_n(a,\vartheta) = a \pm (\phi_o/a\omega)(2n+1) \, |B_n| \, x_b \, j_n'(x_b) \, P_n(\cos\vartheta). \qquad (31)$$

This has the typical shape of a spherical multipole of nth order ; it is plotted (choosing the positive sign) in Fig. 6 for n = 0 (monopole or breathing mode, a radially symmetric in-and-out pulsating motion), n = 1 (dipole or, to first order, rigid back-and-forth motion), n=2 (quadrupole, or alternation between prolate and oblate ellipsoidal shape), and n = 3 (octupole, or pear-shaped deformation). The plots in Fig. 6b are made at the fundamental resonance frequency of each mode[11] (shown in Table I), and in addition at 3% below and above each resonance frequency, respectivley. The scale is arbitrary but is the same for a given value of n. It is seen that no

pronounced (i.e. factors $\sim \rho_w / \rho_b \sim 10^3$) resonant enhancement takes place in the radial displacements of the surface, while some moderate (factors $\lesssim 10$) enhancement does seem to occur.

Mathematically, this arises as follows. As shown in Ref. 11 (Eq. 35), one has at resonance:

$$ j_n' (x_b) = O (\rho_b / \rho_w) , \tag{32} $$

so that B_n in Eq. (31) will be of order $\rho_w / \rho_b \sim 10^3$, while off resonacnce, it is of order unity. However, only the combination $|B_n| j_n' (x_b)$ appears in Eq. (31) so that $R_n (\alpha, \vartheta)$ remains of order unity at resonance and does not show any significant resonance effects. The physical reason for this lies in the boundary condition of continuity of the radial displacement, linking the interior radial motion to that of the external fluid on the boundary. Since only the interior fluid reson tes[23] at the resonance frequencies of the bubble, this linkage prohibits a pronunced resonance motion of the shape of the bubble surface.

We now proceed to plotting the motion of the air particles in the _interior_ of the bubble, and shall find that it is here where the pronounced (order $\rho_w / \rho_b \sim 10^3$) resonance effects occur. This shows clearly that the bubble resonances are resonances of the interior fluid. First, we consider the radial particle displacements inside the bubble which may be described

by the deformation of an originally spherical surface of radius r; this will be changed in the extreme position according to

$$R(r,\vartheta) = r + (\phi_0/a\omega)(2n+1)|B_n| X_b j_n'(k_b r) P_n(\cos\vartheta). \quad (33)$$

In Fig. 7, we plot the quantity R (r,o) $- r$, i.e. the displacement at $\vartheta = 0$ (where it assumes its maximun value since $P_n(1) = 1$) as a function of r. This done for the cases (n, ℓ) equal to (o,1) and (0,2), i.e. monopole fundamental and first overtone (Fig. 7a), further (1,1) and (1,2), i.e. dipole fundamental and first overtone (Fig. 7b), and finally (2,1) and (2,2), i.e. quadrupole fundamental and first overtone (Fig. 7c). As before, the displacement is drawn at the corresponding resonance frequency of Table I, and at a frequency 3% below (-) and above (+) resonance.

The following information is obtained from this figure:

(a) A resonance enhancement takes place in the radial displacement inside the bubble, which is of order $\rho_w/\rho_b \sim 10^3$ (or at least 10^2) while no comparable enhancement occurs at the surface. The fundamental monopole (0,1) is an exception to this.

(b) Not counting any nodes in the low-amplitude portion near the surface, the number of radial nodes N_r in the radial displacement is given by $N_r = \ell - 1$ (the monopole n = 0 being an exception). Generally, N_r is determined by the behavior of

$j'_n (k_b r)$ as a function or r, for k_b at the appropriate resonance frequency.

(c) For higher multipolarity n, the pattern of large radial displacements shifts closer to the surface.

(d) Due to the narrowness of the (n, ℓ) $\neq$ (0 ,1) resonances, a $\pm$ 3% frequency shift brings us well away from the resonance while for the monopole fundamental (0 ,1), it still leaves us high up on its shoulder.

The mention/resonant radial enhancement occurs mathematically because the factor $|B_n|$ in Eq. (33), which shows the mentioned enhancement as the frequency passes through the resonance frequency, is now accompanied by $j'_n(k_b r)$ rather than by $j'_n (x_b)$, and only the latter factor has a compensating minimum at resonance as mentioned above.

In Fig. 8, we present some graphics of the full angular pattern of radial displacements directly at resonance, plotted at originally equidistant radial intervals. This is shown for the case (n,ℓ) = (0,1) and (0,2) in Fig. 8a (monopole fundamental and its first overtone), for (1,1) and (1,2) in Fig. 8b (dipole fundamental and its first overtone), and for (2,1) and (2,2) in Fig. 8c (quadrupole fundamental and its first overtone), indicating the uniform radial shifts that take plance in the fundamental mode and the non-uniform shifts in the overtones.

We finally consider angular displacements of the bubble contents, and the resonance effects that occur in them. From Eqs. (29) and (30), the extreme values of the modal angular displacements of the air particles inside the bubble are obtained as

$$\mu_{\vartheta}^{(n)}(r, \vartheta) = (\phi_0 / r\omega)(2n+1)|B_n| j_n(k_b r) \sin\vartheta \, P_n'(\cos\vartheta). \tag{34}$$

The argument after Eq. (32) now indicates that $u_{\vartheta}^{(n)}(r, \vartheta)$ will also show a resonance enhancement as the frequency passes through the resonance frequency since the coefficient B_n does; the latter is here accompanied in Eq. (34) by the factor $j_n(k_b r)$ which is of order unity throughout, so that unlike $R_n(a, \vartheta)$, the angular particle motion shows a resonance maximum at the resonance frequency even at the bubble surface.

In Fig. 9, we plot $\mu_{\vartheta}^{(n)}(r, \vartheta)$ indicated by arrows, for a number of appropriate values of ϑ and at equidistant radial intervals, for the modes $n = 1$ and 2 (no angular motion takes place for the monopole $n = 0$ which constitutes a radial in-and-out pulsation) at the fundamental resonance frequency of each mode and at the first overtone

frequency.   All scales are relative here.

It is seen that the dipole has angular modes at $\vartheta = 0°$ and $180°$, and maxima at $\vartheta = 90°$ and $270°$; the quadrupole has nodes at $\vartheta = 0°$, $90°$, $180°$ and $270°$ and maxim at $\vartheta = 45°$, $135°$, $225°$ and $315°$. The octupole has nodes at $\vartheta = 0°$, $60°$ etc. and maxima at $30°$, $90°$ etc.

In Fig. 10, we plot the angular displacement of the modes n=1,2 and 3 at the angle of its maximum vs. the radial coordinate ; in Fig. 10 a for the fundamentals of the n = 1,2 and 3 modes, in Fig. 10 b for the first overtones. We also mention that as in the case of the radial displacements, the values of $u_\vartheta^{(n)} (r, \vartheta)$ drop by values of the order 10^{-2} when we move the frequency away by $\pm$ 3% from the resonance frequency; this effect is not graphically represented here.

Figs. 9 and 10 together with what was just said, indicate that as stated above, the angular displacements exhibit resonance effects throughout the interior of the bubble, right up its surface. At that place, the air motion slips against the motion of the water particles which does not show any resonance effects.

Our foregoing discussion of the radial and angular displace-

ments of the air content of a bubble indicates that a resonance
manifests itself here by a violent motion of the air particles
inside the bubble, rather than by a resonant deformation of the
bubble surface. It can be expected that similar results hold
for the interior motion of the elastic medium *in* the case of
resonant sound scattering from a solid object.

IV. Conclusions

We have analyzed the dynamics of the resonant behavior of a penetrable spherical body which is subjected to an incident plane acoustic wave, in terms of circumferential waves as described by Regge pole theory. Considering the air-filled spherical bubble immersed in water as an example, it was shown that an infinite set of Regge poles labeled by $\ell = 0,1,2...$, moving along trajectories in the complex n-plane with increasing frequency, generate in succession the fundamental ($\ell = 0$) and overtone ($\ell \geq 1$) modal resonances of succesively higher multipolarity n every time a pole moves past the integer value n.

We have shown that the Regge poles cause the appareance of circumferential surface (or tidal) waves on the sphere that are generated due to the action of the impinging sound, but which could equally well have been created by a more general external force since they are a property of the scattering object and not of the particular excitation mechanism. The occurence of the resonances themselves was then recongnized to take place at frequency at which an integer-plus-half number of wavelengths (the integer being equal to the multipolarity n

of the collective bubble vibration) could fit over the sphere's circumference, so that the phase matching of the repeatedly circumnavigating surface waves (taking into account a phase jump of $-\pi/2$ of the surface waves when passing through each of the convergence zones at the north and south pole) will lead to their resonant reinforcement.

Graphical illustrations were presented for the propagation of these surface waves, as well as of the modal surface deformation and of the gas motion inside the bubble. The latter manifestly exhibit the resonance effects, while the surface deformations do not, on account of the boundary conditions.

The here-analyzed dynamic effects around spherical gas bubbles in water are expected to be of very general validity, and to be applicable to spherical scatterers of much more general nature (e.g., elastic bodies in fluids, fluid-filled[23] cavities or solid inclusions in an elastic medium[24] etc.) In fact, we have been able to describe[25] in very similar terms the phenomenon of the giant collective resonances of atomic nuclei which, on the basis of a hydrodynamical model of the nucleus, may also be thought

of being caused by the phase matching of circumferential
"nuclear tidal waves" generated by various kinds of nuclear
reactions.

Acknowledgements

Table I

Resonance frequencies $x_{n\ell}$ of the fundamental ($\ell = 1$)
and overtones ($\ell = 2, 3, \ldots$) of the lowest multipole resonances
($n = 0 \ldots 4$) of an air-bubble in water.

multipole	ℓ / n	1	2	3	4	5	6
monopole	0	0.01391	1.0161	1.7467	2.4658	3.1792	3.8938
dipole	1	0.4712	1.3433	2.0817	2.80504	3.5229	—
quadrupole	2	0.7555	1.6485	2.4000	3.1311	3.8539	—
octupole	3	1.0214	1.9411	2.7074	3.4478	—	—

References

1. H. Überall, L. R. Dragonette, and L. Flax, "Relation Between Creeping Waves and Normal Modes of Vibration of a Curved Body," J. Acoust. Soc. Am. 61, 711-715 (1977).

2. J. W. Dickey and H. Überall, "Surface Wave Resonances in Sound Scattering from Elastic Cylinders", J. Acoust. Soc. Am. 63, 319-320 (1978); J. W. Dickey, Ph.D. dissertation, The Catholic University of America, Washington, D.C., 1977.

3. L. Flax, L. R. Dragonette, and H. Überall, "Theory of Elastic Resonance Excitation by Sound Scattering", J. Acoust. Soc. Am. 63, 723-731 (1968); L. R. Dragonette, Ph.D. dissertation, The Catholic University of America, Washington, D.C., 1978.

4. J. D. Murphy, E. D. Breitenbach, and H. Überall, "Resonance Scattering of Acoustic Waves from Cylindrical Shells", J. Acoust. Soc. Am. 64, 677 (1978)

5. J. D. Murphy, J. George, and H. Überall, "Isolation of the Resonant Component in Acoustic Scattering from Fluid-Loaded Cylindrical Shells" (submitted to J. Wave Motion).

6. A. J. Haug, S. G. Solomon, and H. Überall, "Resonance Theory of Elastic Wave Scattering from a Cylindrical Cavity", J. Sound Vib. 57 51-58 (1978)

7. G. C. Gaunaurd and H. Überall, "Scattering of Dilatational Waves Incident on a Resonating Fluid-Filled Spherical Cavity Inside a Sound-Absorbing Material", J. Acoust. Soc. Am. 63, S40, 1978; also, "Theory of Resonant Scattering from Spherical Cavities in Elastic and Viscoelastic Media, J. Acoust. Soc. Am. 63, 1699 (1978)

8. G. C. Gaunaurd, K. P. Scharnhorst, and H. Überall, "A New Method to Determine Shear-Absorption Using the Viscoelasto-dynamic Resonance Scattering Formalism", J. Acoust. Soc. Am. 64, 1211 (1978)

9. G. C. Gaunaurd, K. P. Scharnhorst, and H. Überall, "Giant Monopole Resonances in the Scattering of Waves From Gas-Filled Spherical Cavities and Bubbles", submitted to J. Acoust. Soc. Am. 64, (1978)

10. See also H. Überall, "Modal and Surface Wave Resonances in Acoustic-Wave Scattering from Elastic Objects, and in Elastic-Wave Scattering from Cavities", Dept. of Physics, Catholic University of America Report, Oct. 21,1977, and Proceedings of the IUTAM Symposium on Modern Problems in Elastic Wave Propagation (J. Miklowitz, ed.), Northwestern Univ., Evanston, Illinois, Sept. 1977.

11. K. A. Sage, J. George, and H. Überall, "Multipole Resonances
     in Sound Scattering from Gas Bubbles in a Liquid," in "High
     Frequency Underwater Acoustic Backscattering", Center for Applied
     Research, School of Engineering and Architecture, Catholic Univer-
     sity of America Report, Dec. 15, 1977, and   submitted to
     J. Acoust. Soc. Am.

12. M. Strasberg, "Gas Bubbles as Sources of Sound in Liquids",
     J. Acoust. Soc. Am. 28, 20-26 (1956).

13. See, e.g., H. Medwin, "Acoustic Probing for Microbubbles at
     Sea", in "Proceedings of the Conference on Oceanic Acoustic
     Modelling, Nr. 17, Part 2, SACLANTCEN, La Spezia, Italy, 1975.

14. See, e.g., R. G. Newton, Scattering Theory of Waves and Particles,
     McGraw-Hill, New York 1966.

15. W. Franz, "Über die Greenschen Funktionen des Zylinders und
     der Kugel," Z. Naturforsch. A9, 705-716 (1954).

16. B. van der Pol and H. Bremmer, "The Diffraction of Electro-
     magnetic Waves from an Electrical Point Source Round   Finitely
     Conducting Sphere, with Applications to Radiotelegraphy   and
     the Theory of the Rainbow," Phil. Mag (7) 24, Part I, 141-176 (1937);
     Part II, Phil. Mag. (7) 24, 825-864 (1937).

17. M. C. Junger and D. Feit, "High-Frequency Response of Point-
     Excited Submerged Spherical Shells", J. Acoust. Soc. Am. 45,
     630-636 (1969).

18. With $0 < \vartheta < \pi$, the continuous propagation of a given circum-
    ferential wave through angular intervals of length π is described
    by the sequence $I(\pi - \vartheta, 0)$, $II(\pi + \vartheta, 1)$, $I(3\pi - \vartheta, 1)$,
    $II(3\pi + \vartheta, 2)$, $I(5\pi - \vartheta, 2)$ ..., where $I(\beta, m)$
    or $II(\beta, m)$ indicate the first ($\varepsilon = 1$) or second ($\varepsilon = -1$),
    exponential in Eq. (19), respectively, β being the continuously
    increasing phase angle around the sphere.

19. See, e.g., I. M. Blatstein, A. V. Newman, and H. Überall,
    "A Comparison of Ray Theory, Modified Ray Theory, and Normal
    Mode Theory for a Deep-Ocean Arbitrary Velocity Profile,"
    J. Acoust. Soc. Am. 55, 1336-1338 (1974).

20. R. C. Fuller and K. W. McVoy, "Regge-Pole Dominance in a Heavy-
    Ion DWBA Calculation", Phys. Lett. 55B, 121-124 (1975).

21. R. Fiorito and H. Überall, "Resonance Theory of Acoustic Reflection
    and Transmission Through a Fluid Layer", submitted to J. Acoust.
    Soc. Am.

22. See. e.g., M. Abramowitz and I. A. Stegun, Handbook of
    Mathematical Functions, Dover, New York, 1965.

23. Reference 11 indicated the bubble multipole resonances to be
    caused by or resonating content of the bubble, since the
    resonances in the partial waves appear superimposed upon a
    background which conicides with the scattering amplitudes for
    an empty (pressure release) sphere. The resonance effect
    just noted in the interior radial particle motion confirms this
    interpretation, and a similar effect is seen below to take place
    in the angular particle motion also.

Figure Captions

Fig. 1. Moduli of individual partial-wave backscattering amplitudes $\left| f_n(\vartheta = \pi) \right|$ $(n = 0 \ldots \ldots 3)$ plotted vs. ka for an air bubble in water, showing resonances superimposed upon a smooth background.

Fig. 2. The nth (here sketched as 2nd) normal mode vibration decomposed in a pair of traveling waves with phase velocities c_n and surface waves labeled by ℓ, with phase velocities c_ℓ.

Fig. 3. (a) Phase velocities c_ℓ of surface waves $\ell = 1$ through 14 as a function of $x \equiv ka$ (dispersion curves) relative to sound velocity in water, c, for an air-filled bubble in water. (b) Group velocities c_ℓ^{gr}/c of the same surface waves.

Fig. 4. (a) Surface wave amplitude on a sphere slightly below a resonance ($n_\ell = 4.7$), with no phase matching. Quarter-wavelength phase jumps at the poles are evident. (b) Surface wave at the $n_\ell = 5$ resonance, with phase matching. Solid line: asymptotic calculation; dashed line: exact calculation. The heavy curves disregard, and the light curves retain, the convergence factor $(\sin \vartheta)^{-1/2}$.

Fig. 5. Same as Fig. 4, for (a) $n_\ell = 0.7$ and (b) $n_\ell = 1$.

Fig. 6.   Surface displacements of an air bubble in water, set into

oscillation by impinging sound, for the modes (a) n = 0

(monopole or breathing mode), (b) n = 1 (dipole), (c)

n = 2 (quadrupole) and (d) n = 3 (octupole). Plots

are at: 3% below the fundamental resonance frequency

given in Table I;   at the resonance frequency, and

at 3% above the resonance frequency   (fundamentals

only). Scales are arbitrary, but are the same for a

given value of n.

Fig. 7.   Radial displacements inside the bubble as functions

of r, at the appropriate resonance frequency as well as

3% below (-) and above (+) the latter: (a) for

monopole fundamental (0,1) and its first overtone (0,2),

(b) for dipole fundamental (1,1) and its first

overtone (1,2), and (c) for quadrupole fundamental

(2,1) and its first overtone (2). Scales are arbitrary,

but are the same for a given (n,ℓ).

Fig. 8.   Resonant displacement of originally equidistant spherical

surfaces inside the bubble, plotted at the resonance

frequency for (a) the monopole fundamental (n,ℓ) = (0,1)

and first overtone (0,2), (b) the dipole fundamental

(n,ℓ) = (1,1) and first overtone (1,2), and (c) the

quadrupole fundamental (2,1) and first overtone (2,2); arbitrary scales.

Fig.9.   Angular displacements $u_\vartheta (r,\vartheta)$ indicated by arrows (arbitrary scale) for $n = 1$ and 2 at the fundamental resonance frequency, i.e. (1,1) and (2,1), and at the first overtone, i. e. (2,1) and (2,2).

Fig. 10. Angular displacements $u_\vartheta (r,\vartheta)$ of the modes $n = 1$, 2 and 3 vs. r/a, each taken at the angle ϑ at which maximum displacement occurs.

Fig. 1
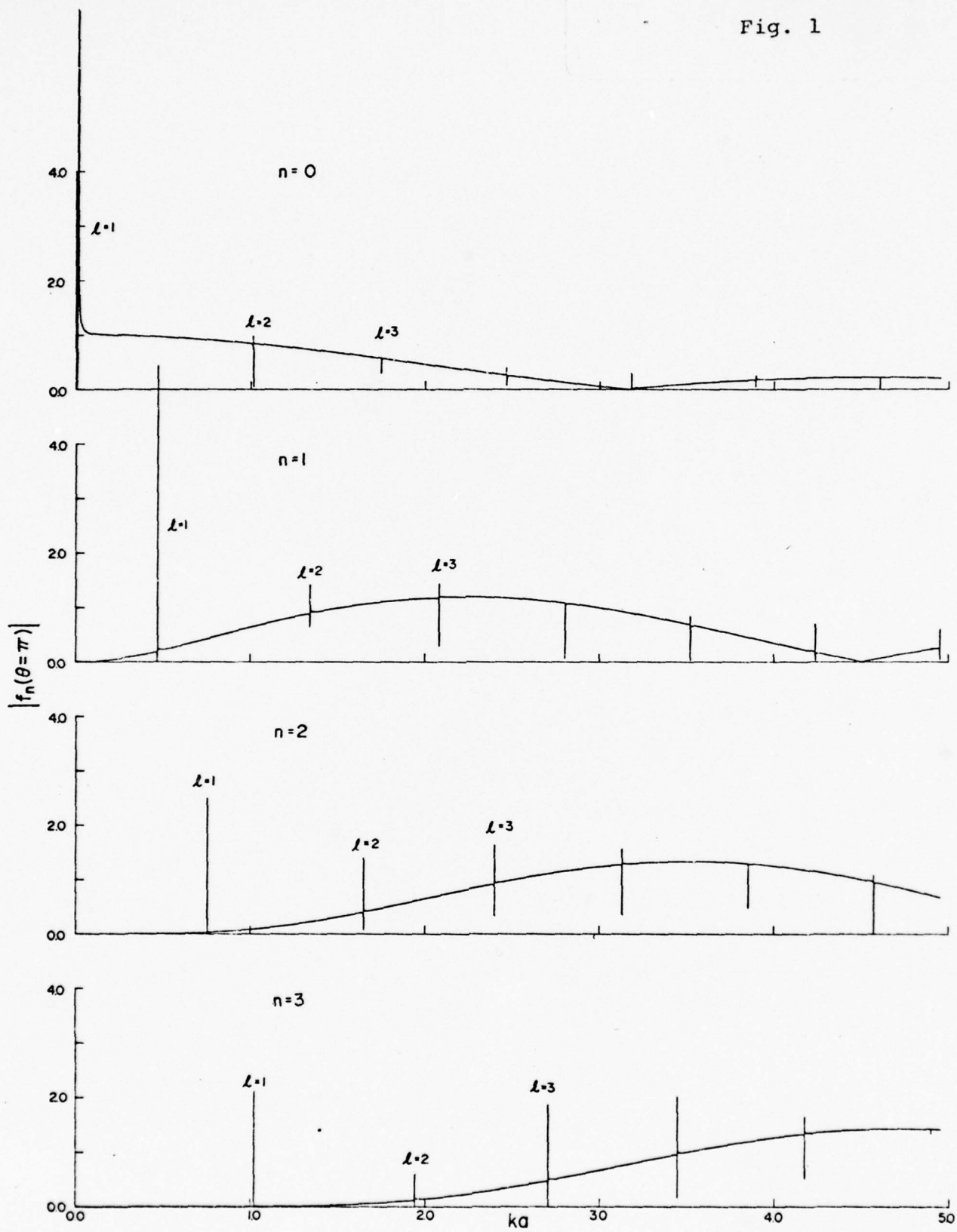
Fig. 2
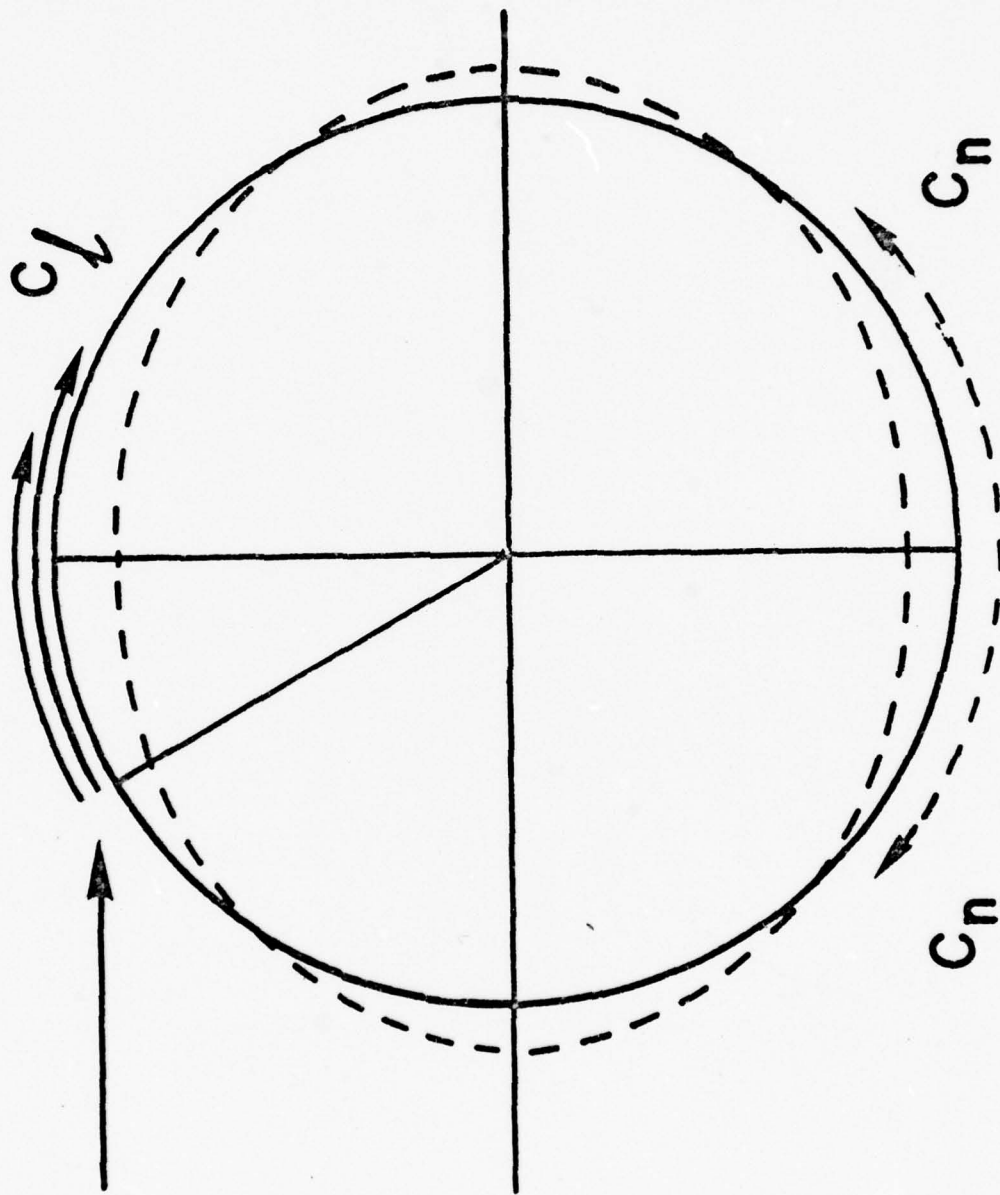
Fig. 4a
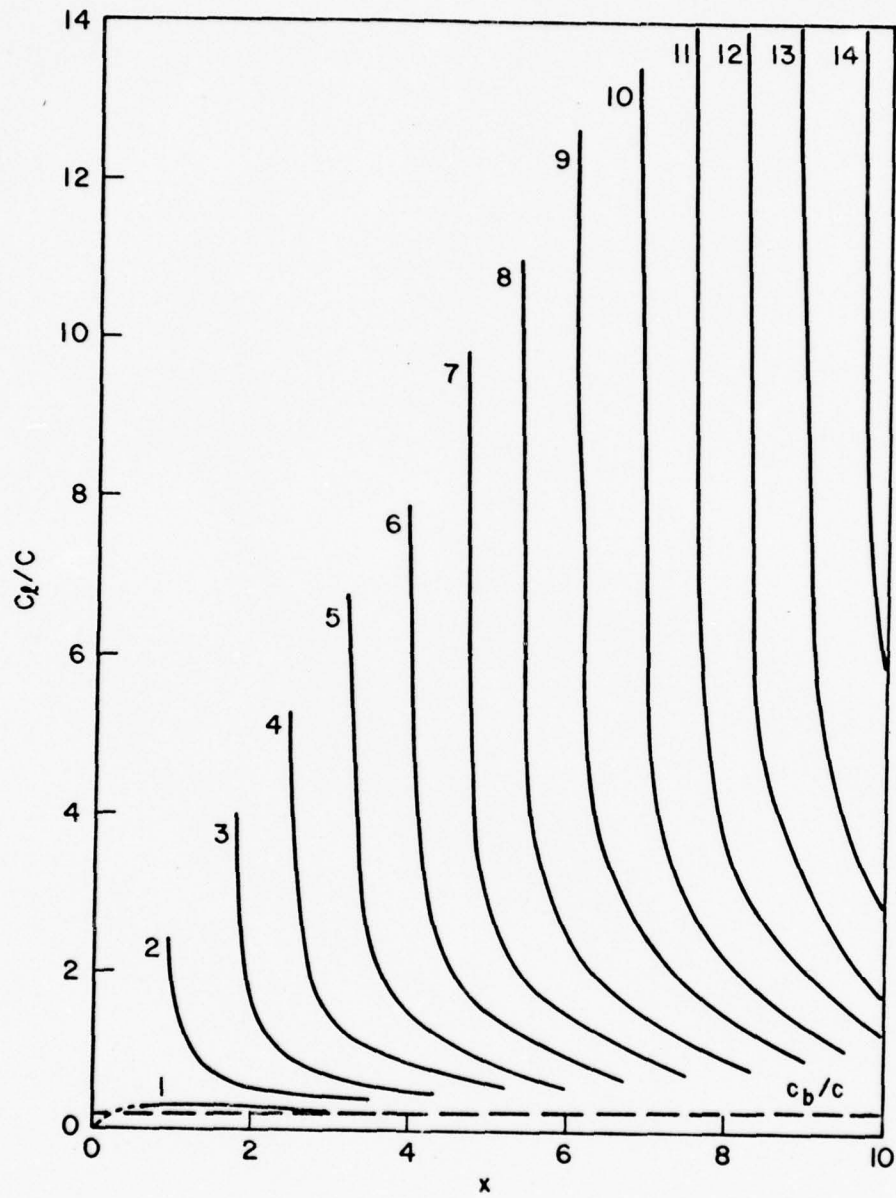
Fig. 5b

res

−3%   +3%

r = a

n = 0

-3%   +3%   r = a   res

n = 1

res +3% r = a

-3%

n = 2

Fig. 6d

Fig. 7a
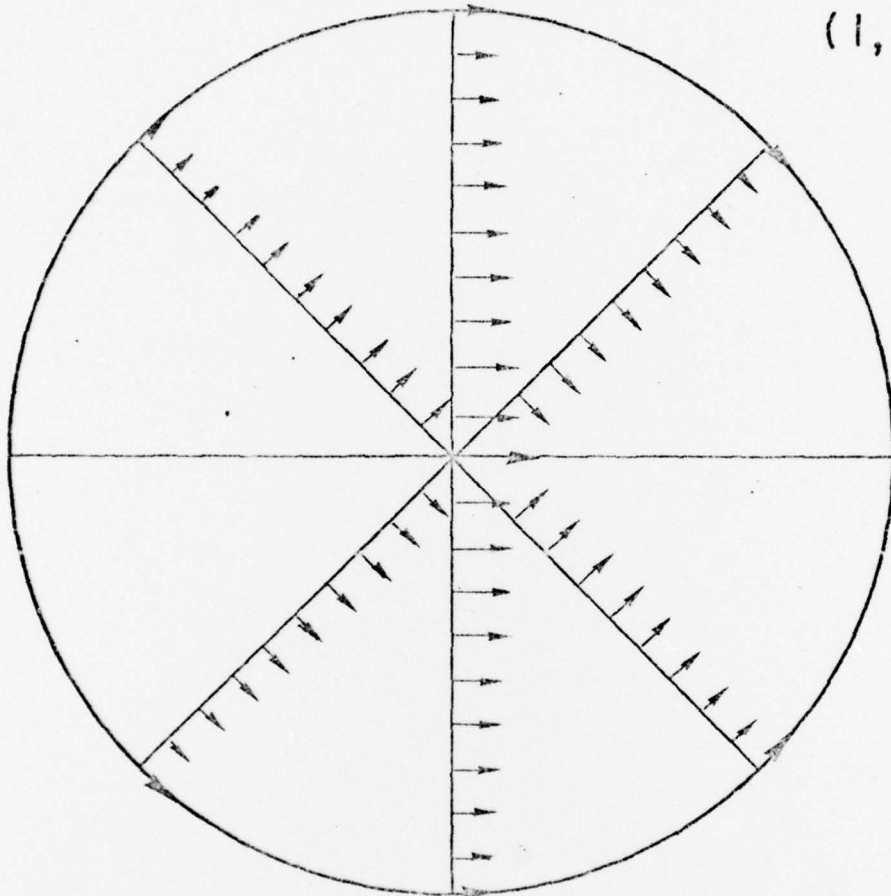
Fig. 70

(0,1)

(0,2)

(1,1)

(1,2)

(2,1)

Fig. 8c
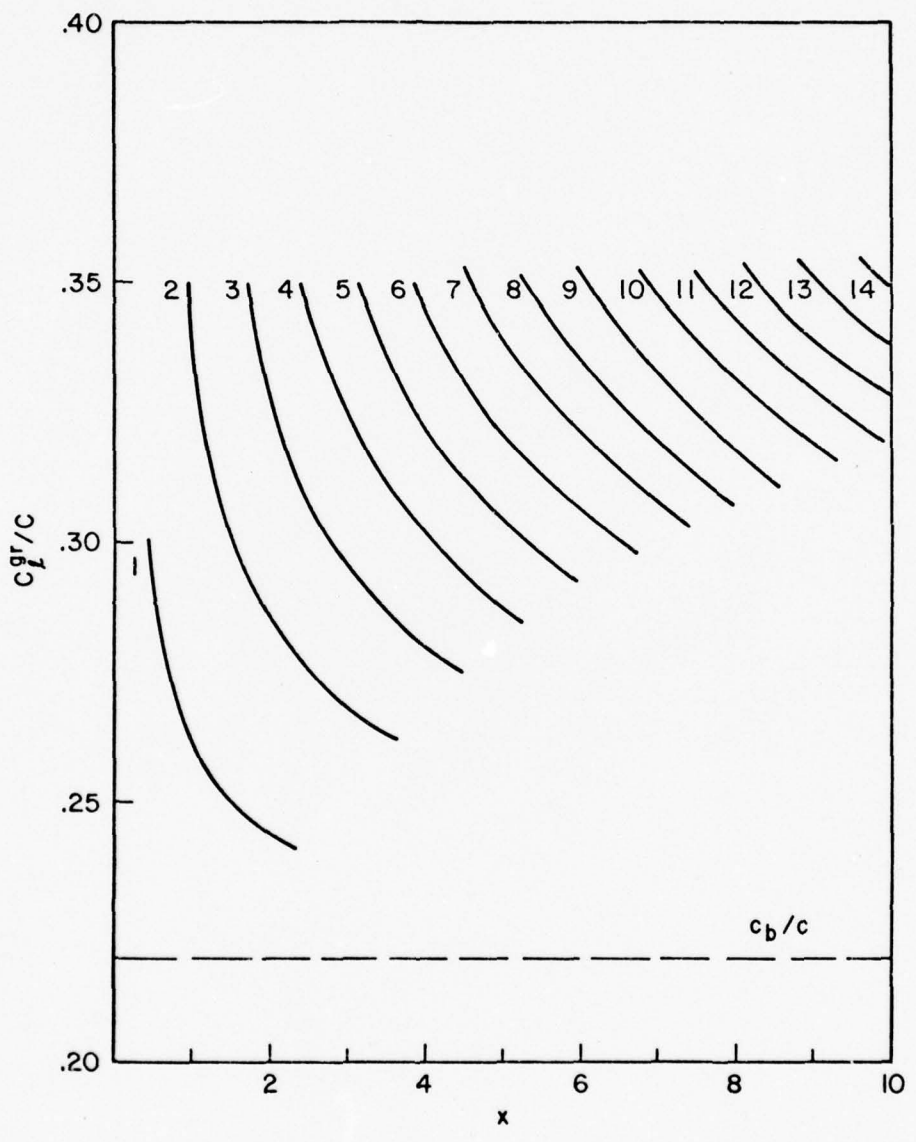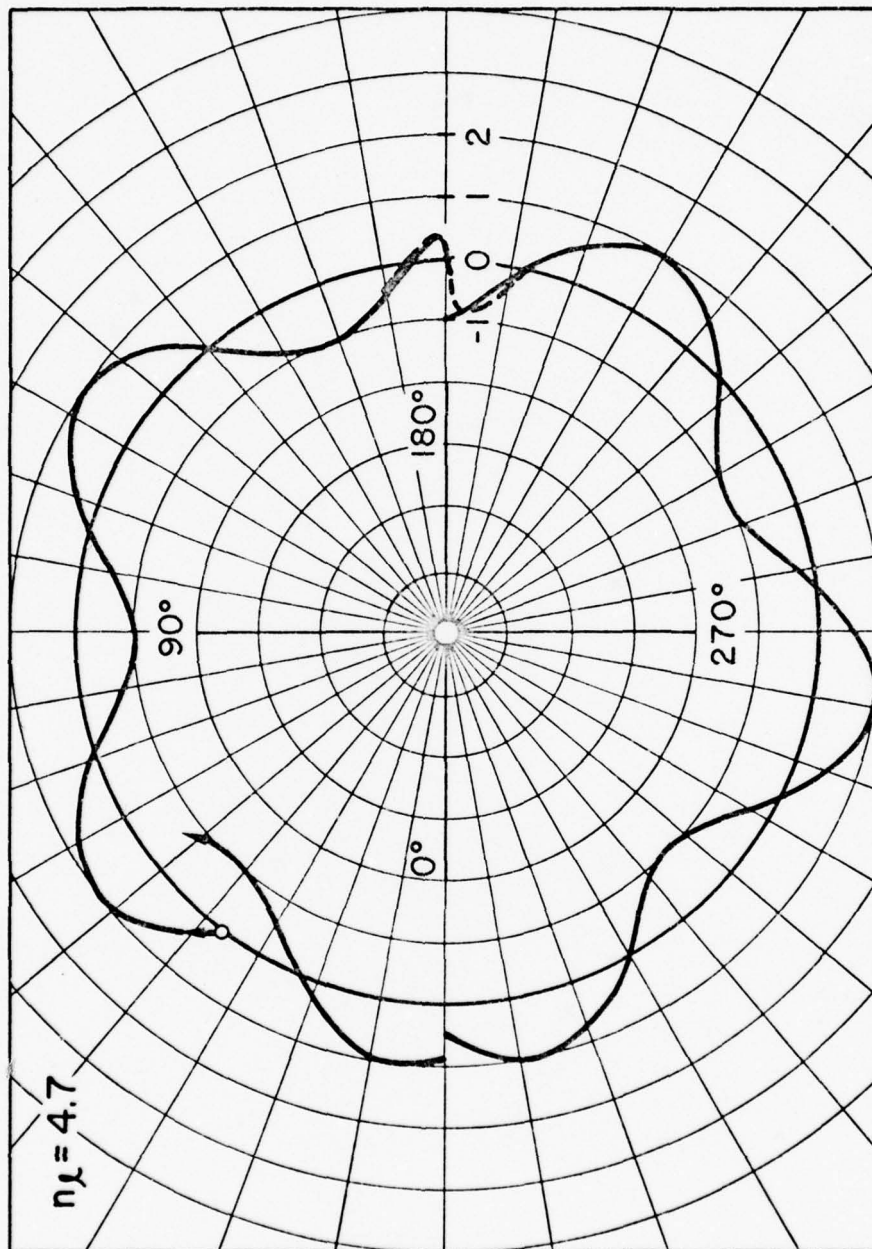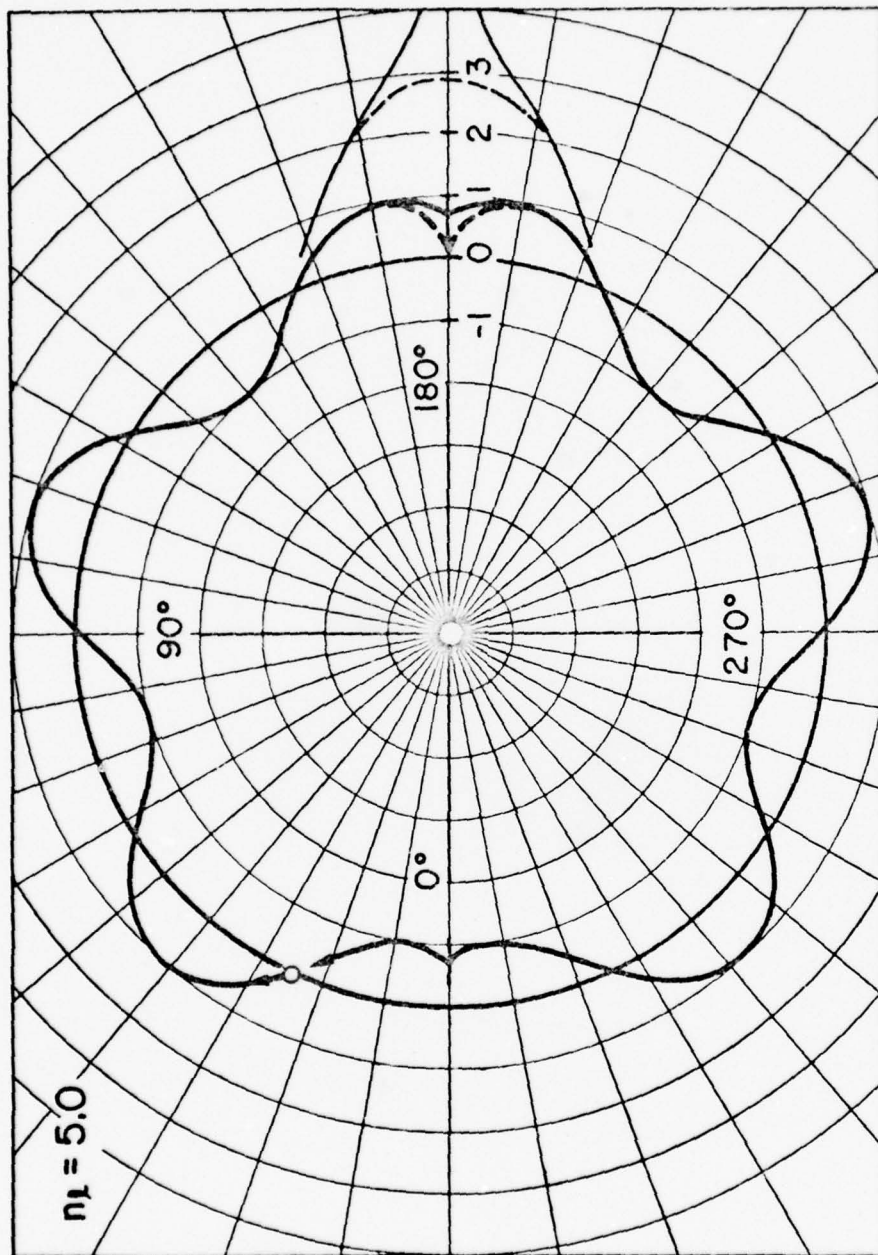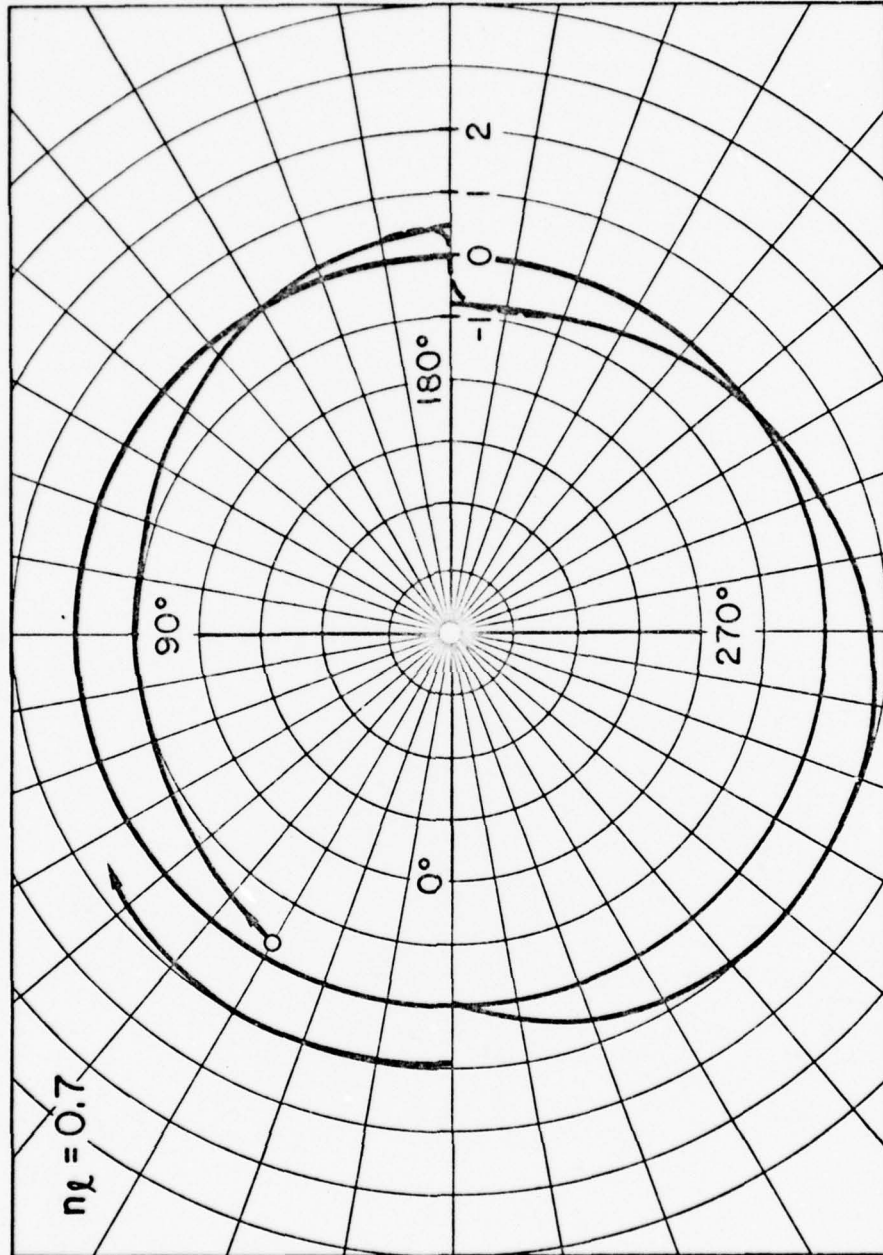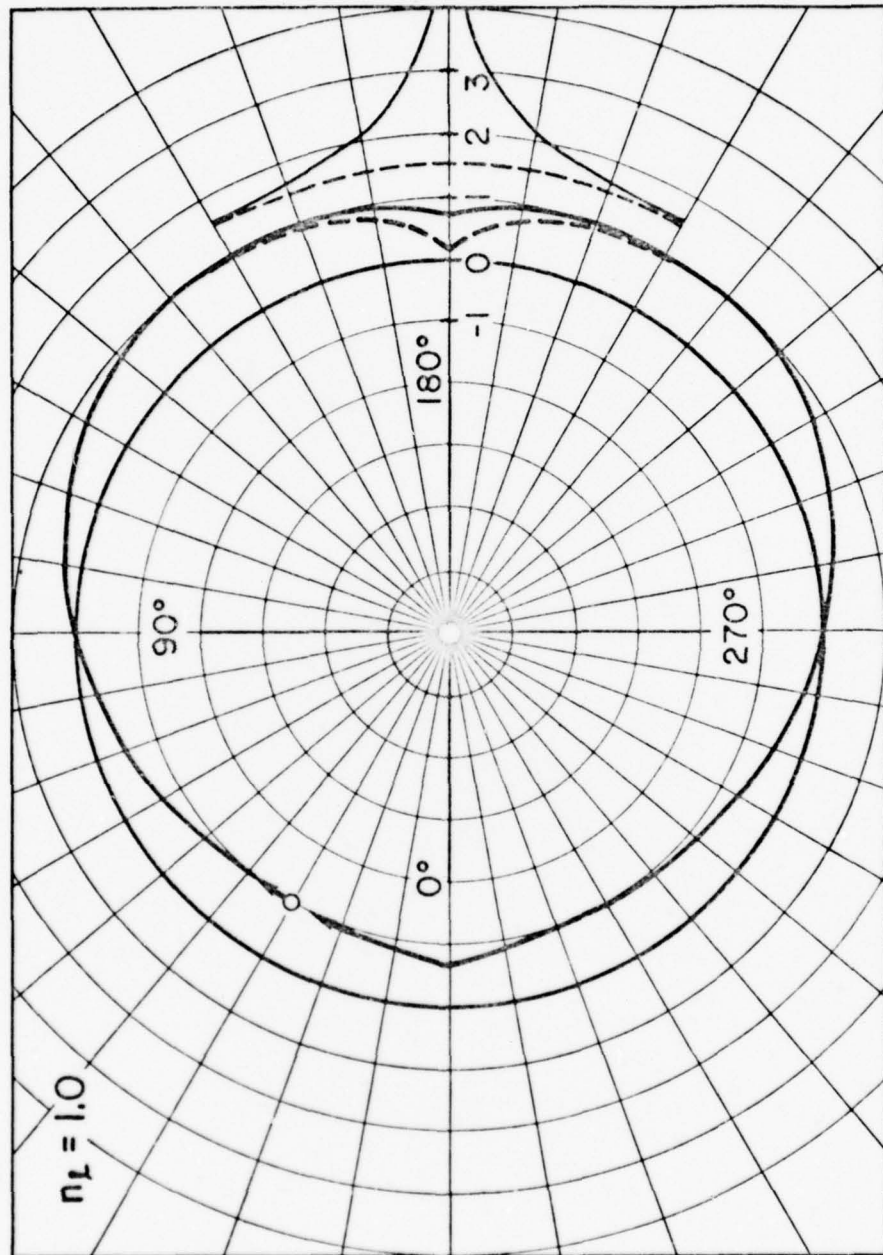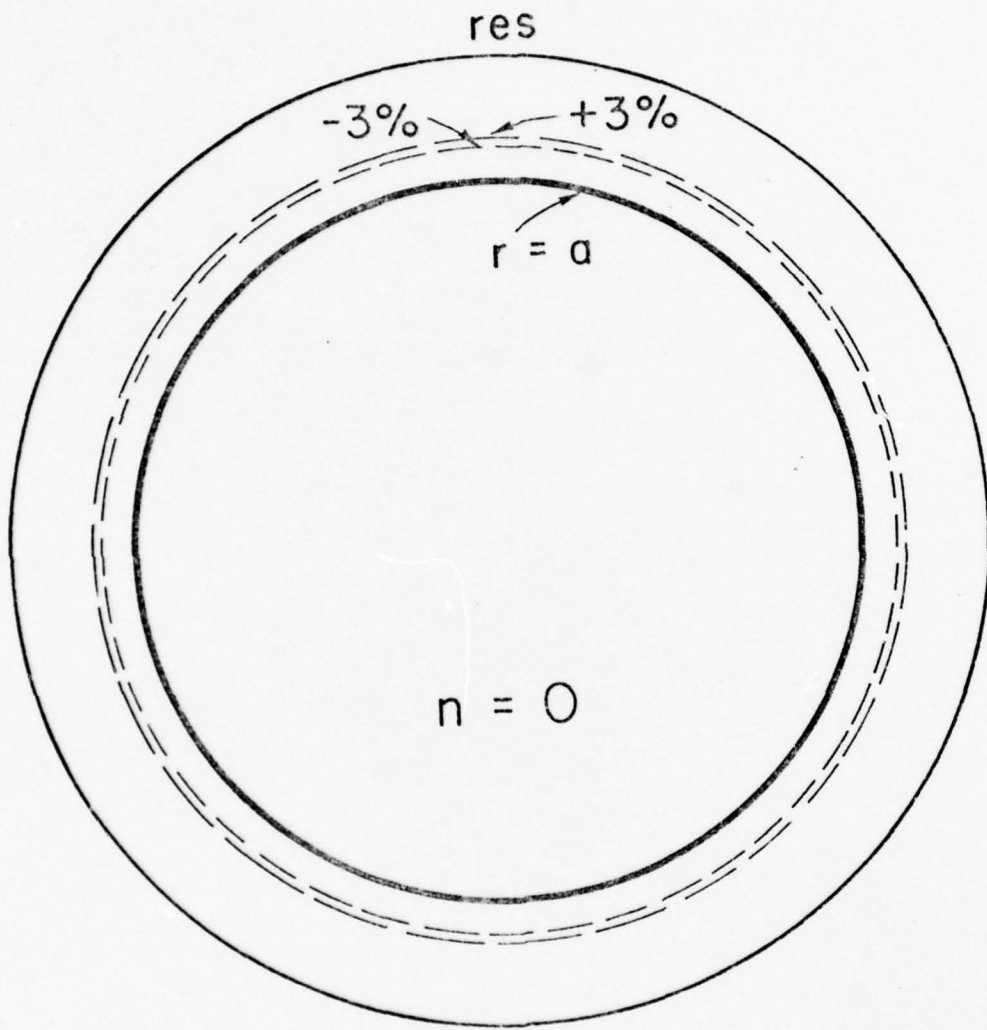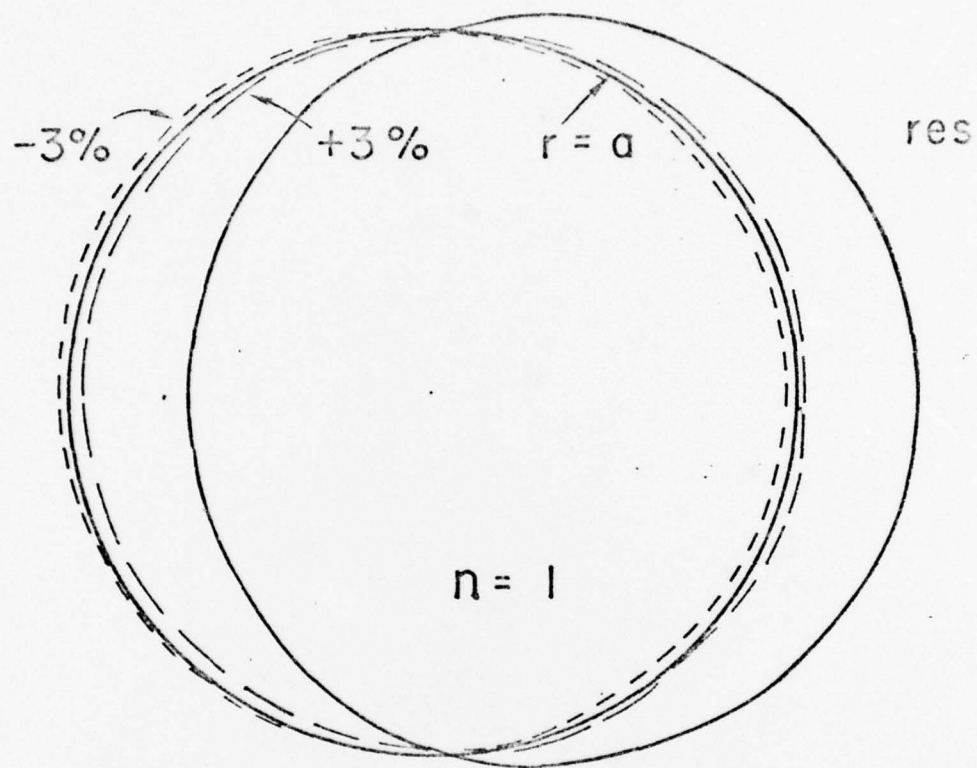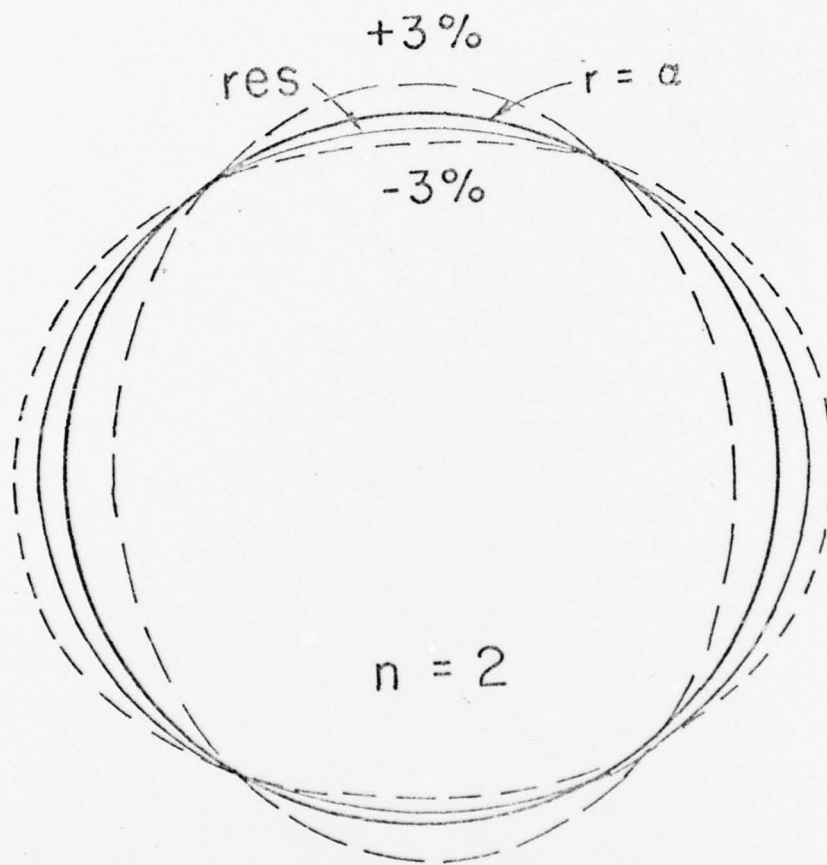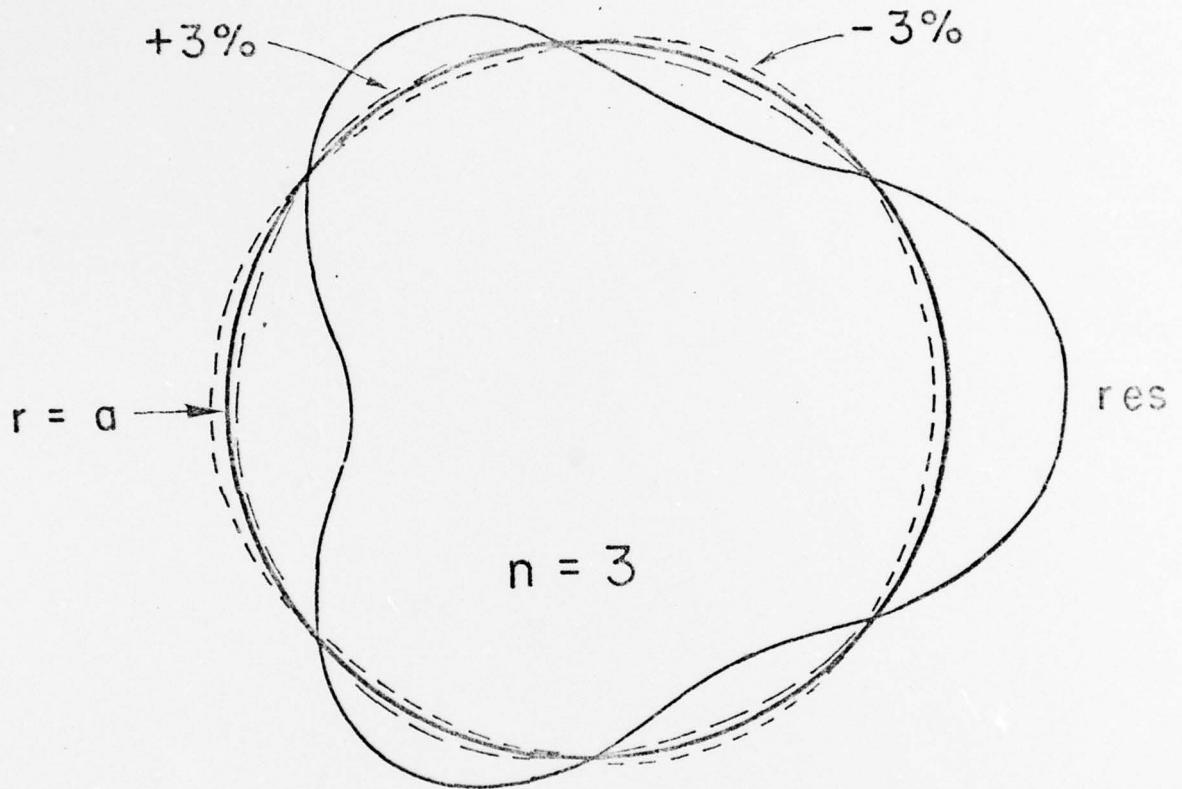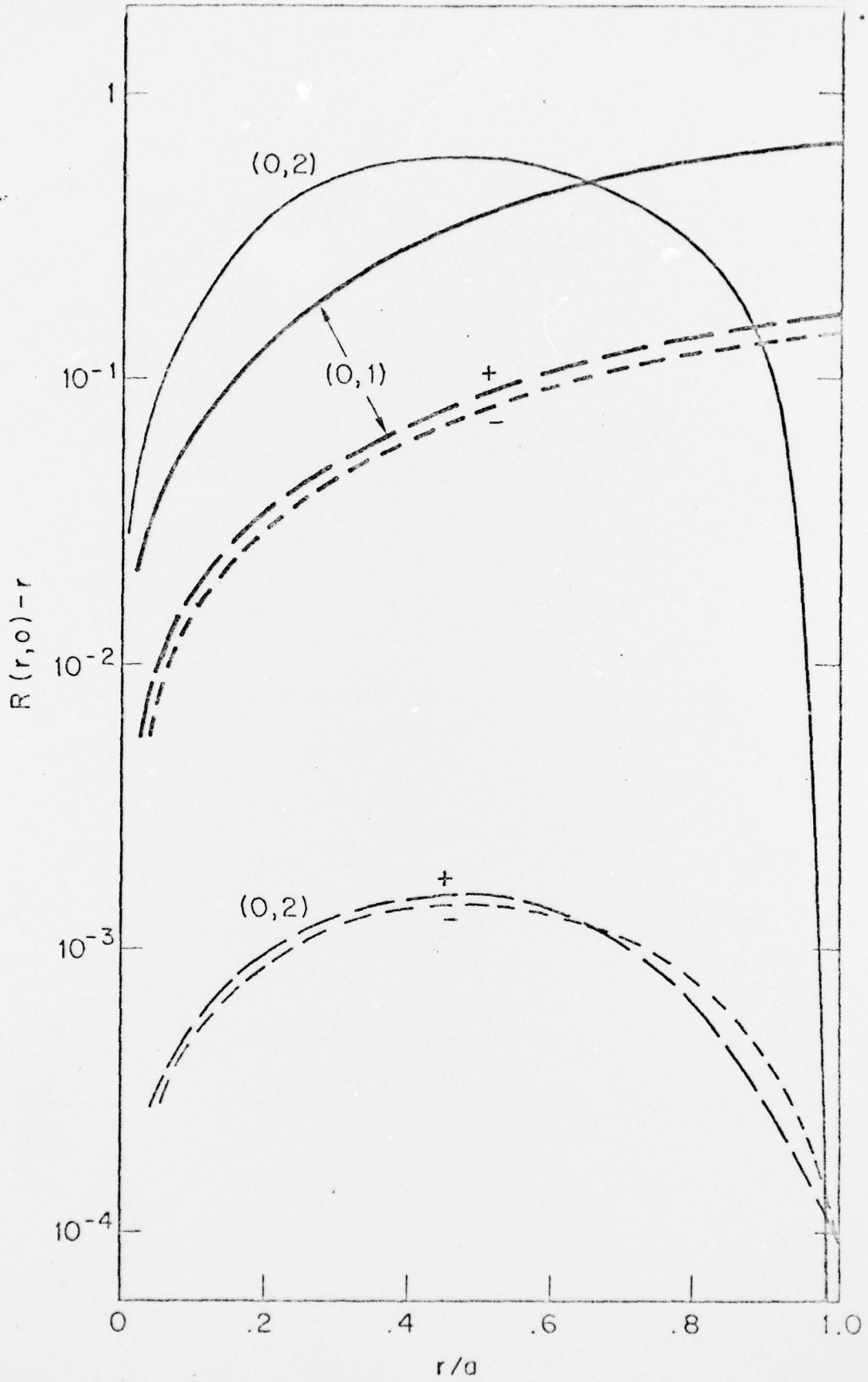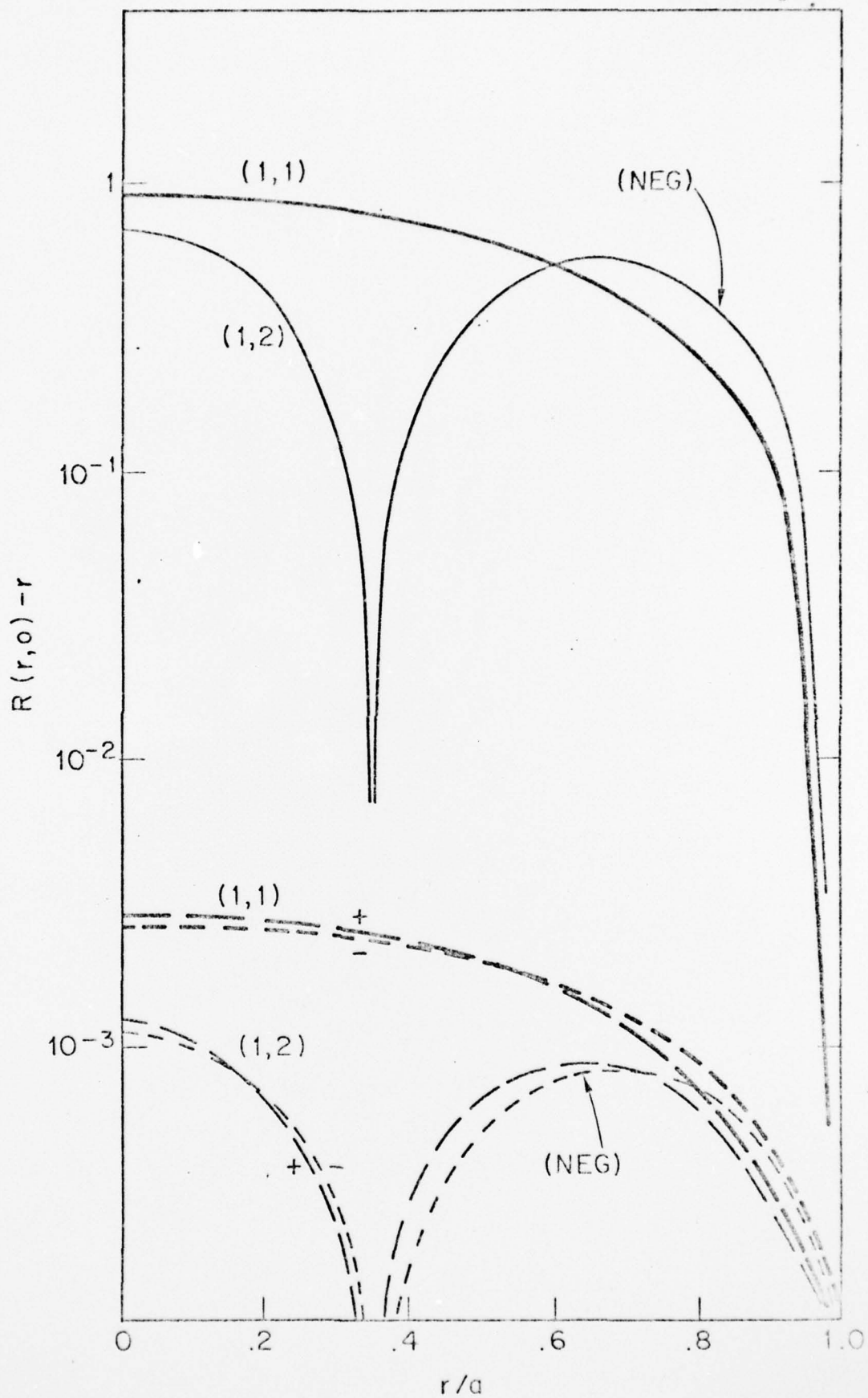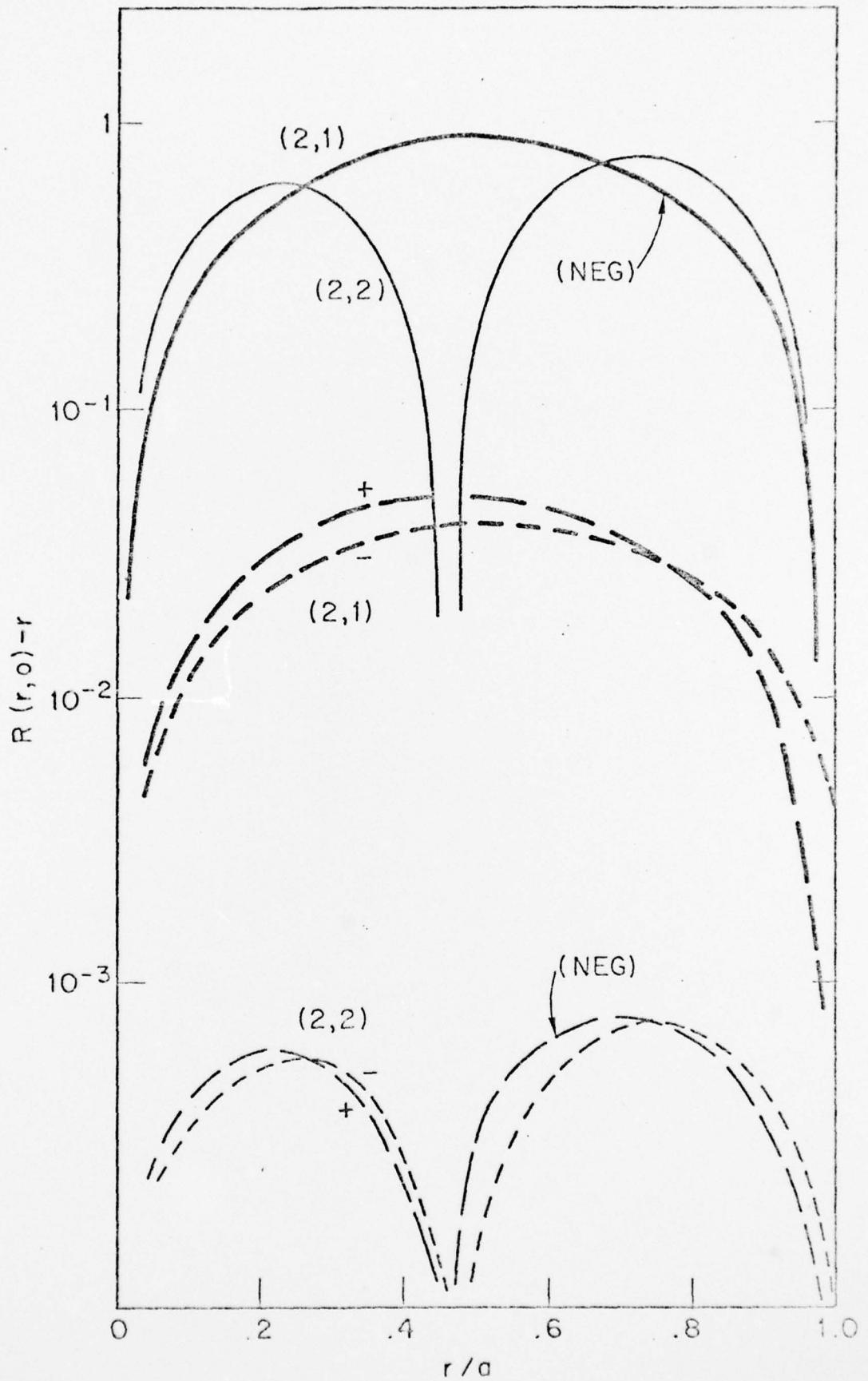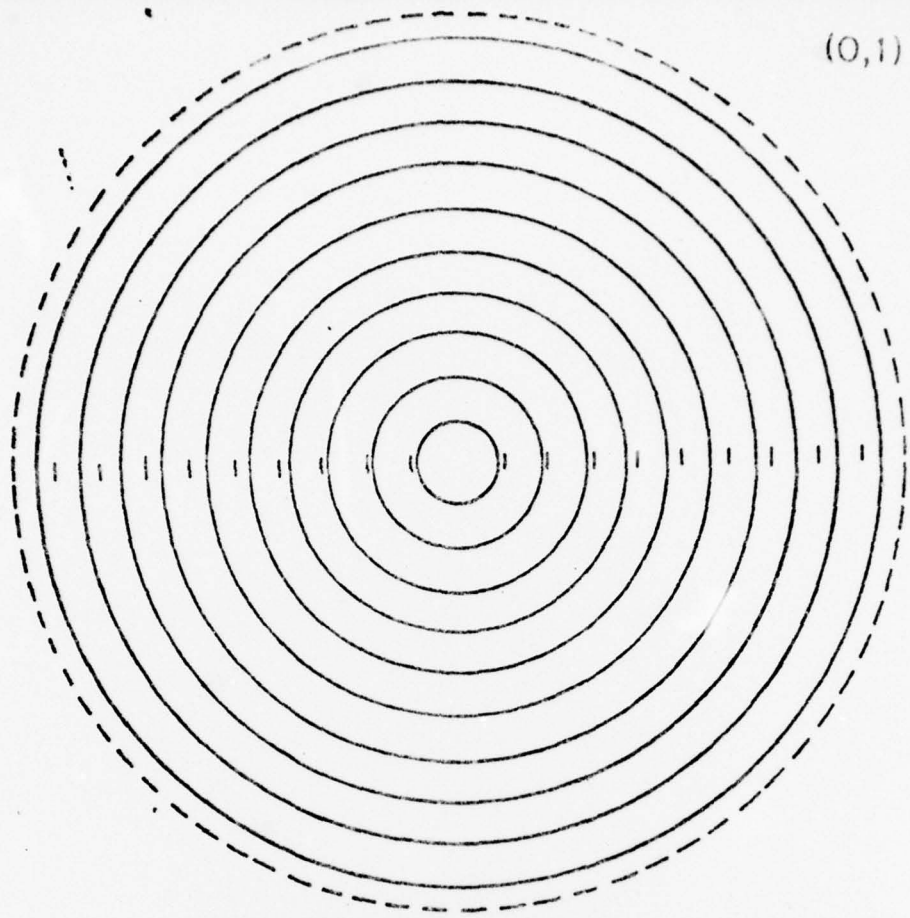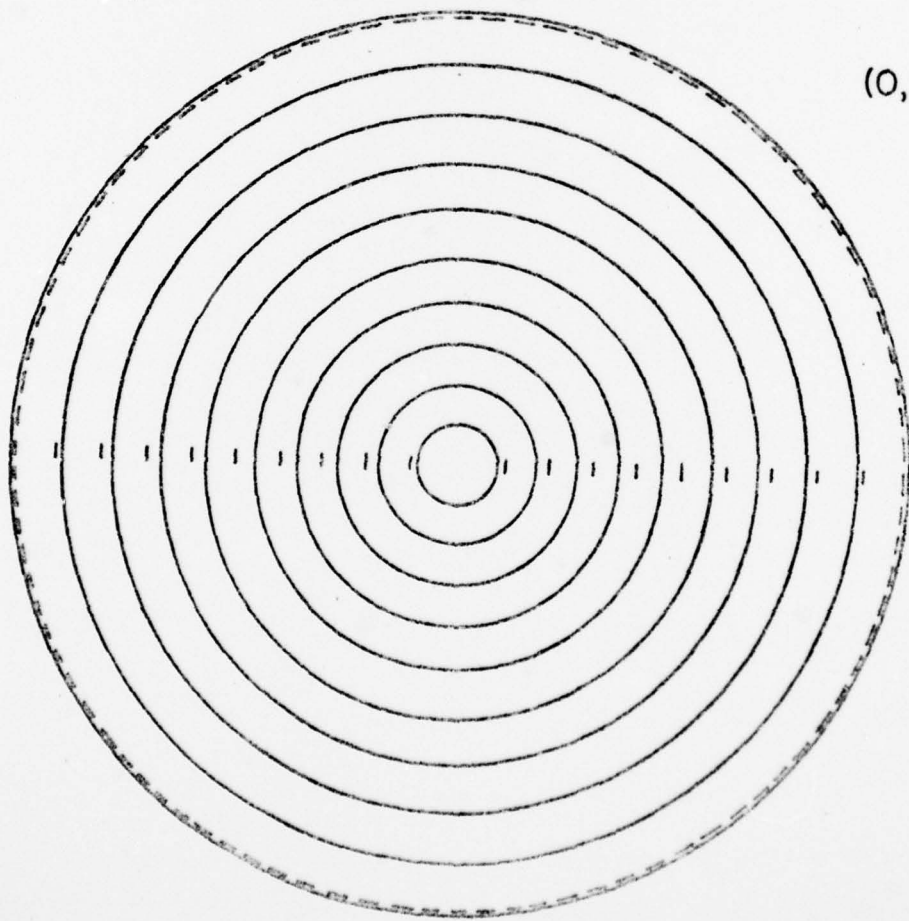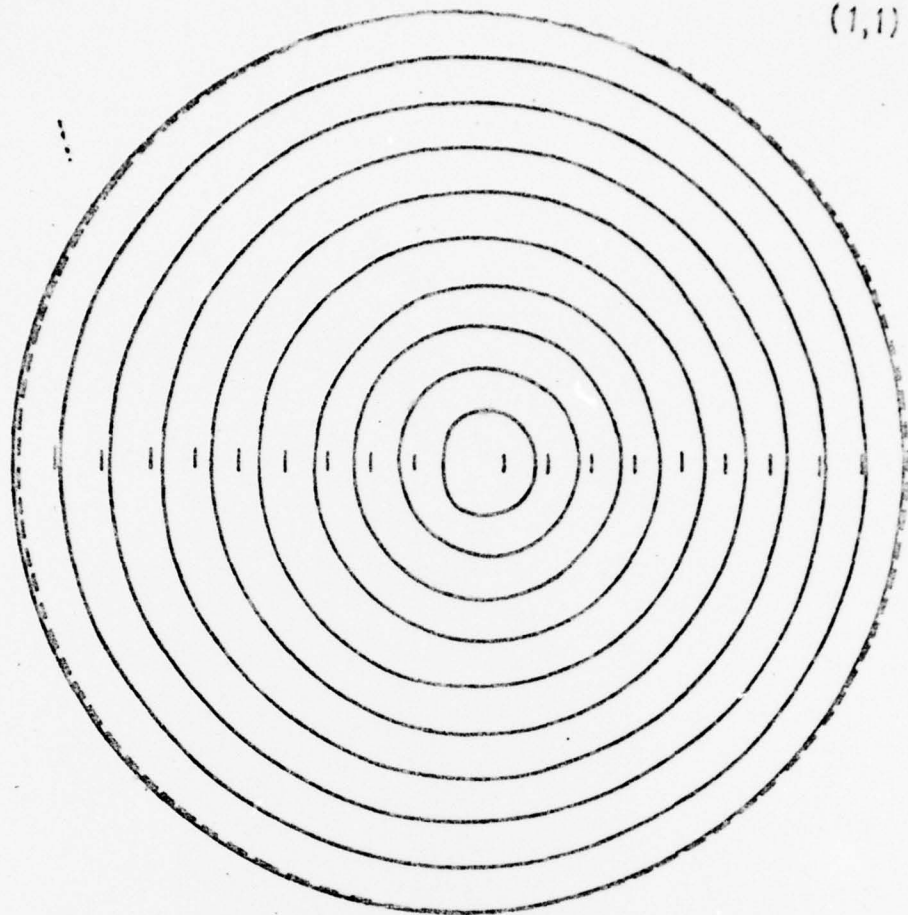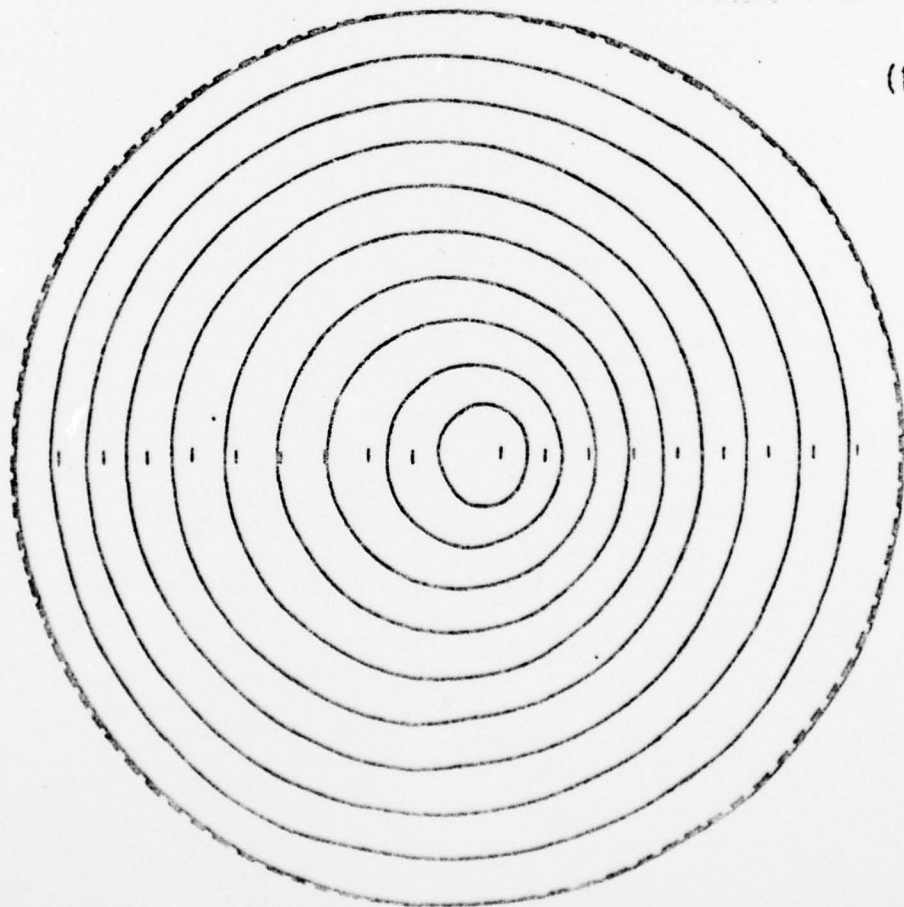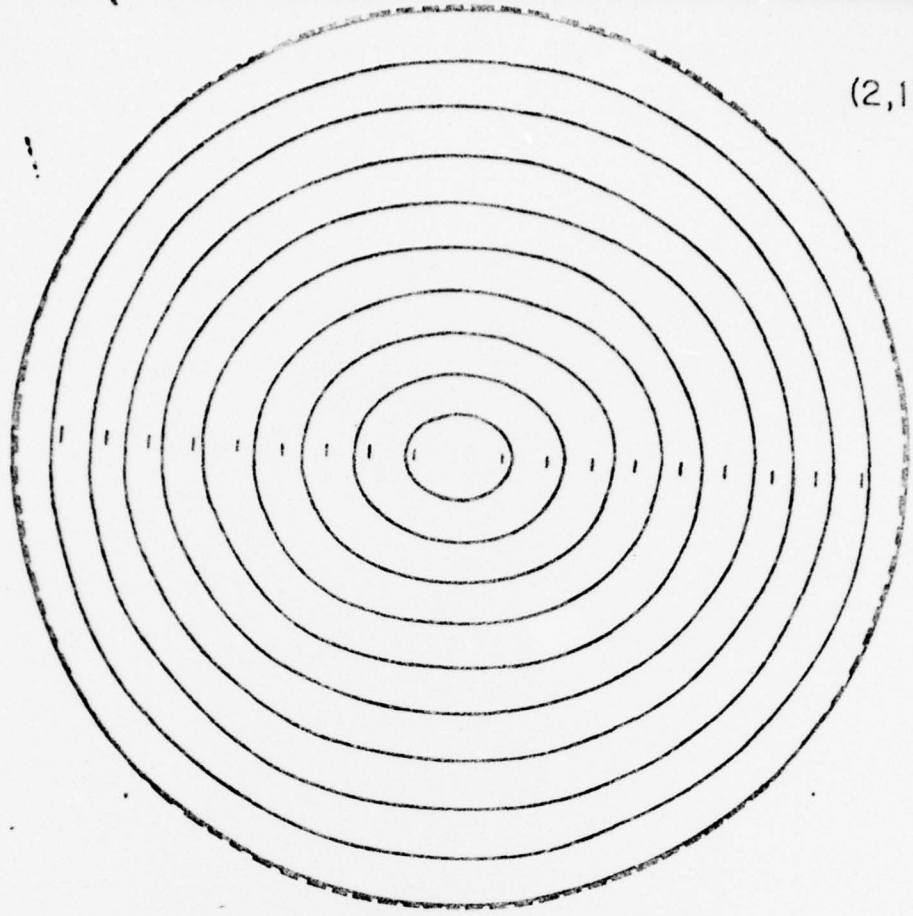
(2,2)
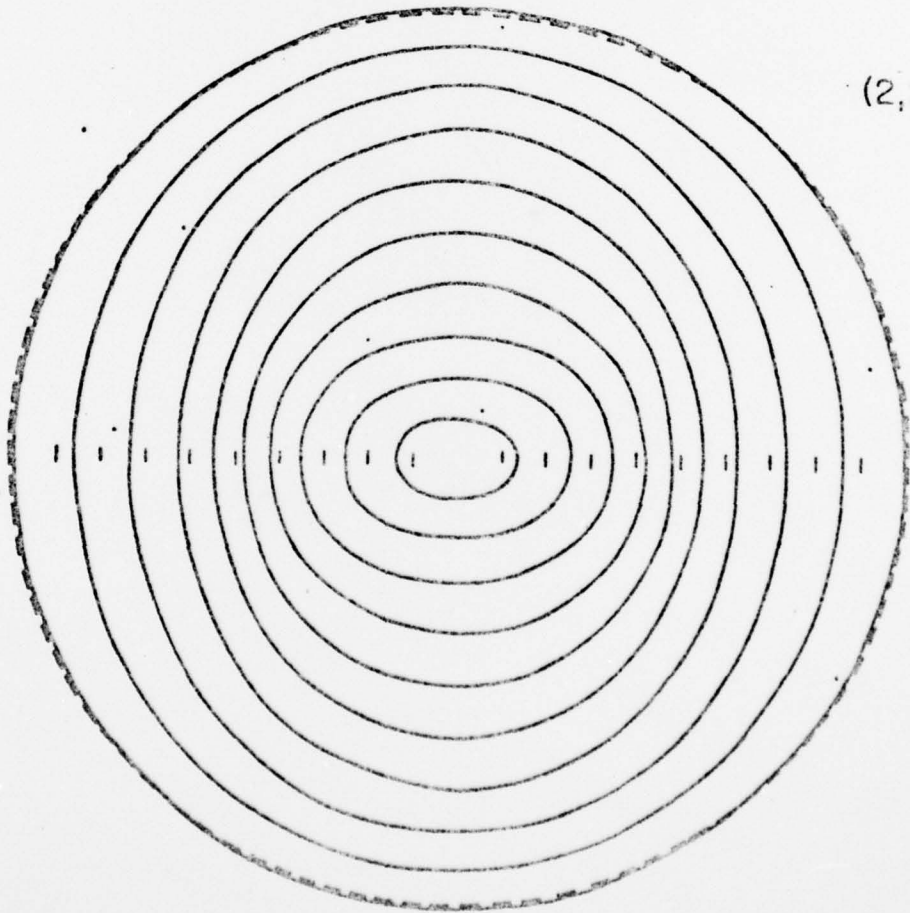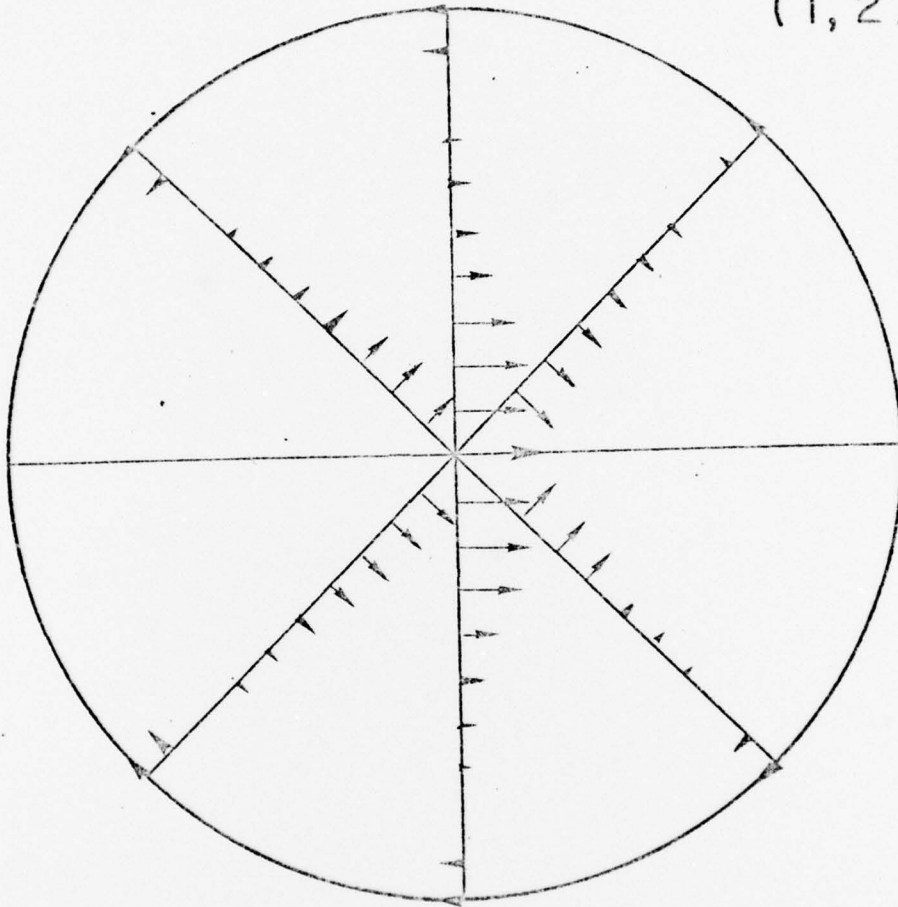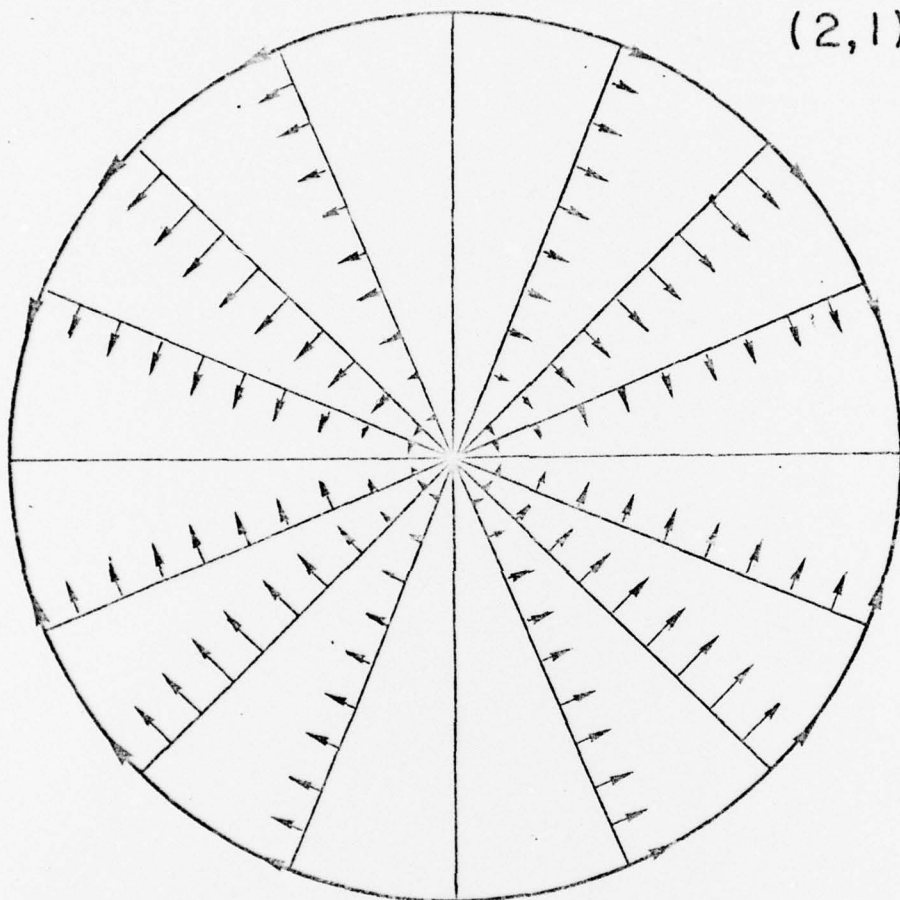
Fig. 9
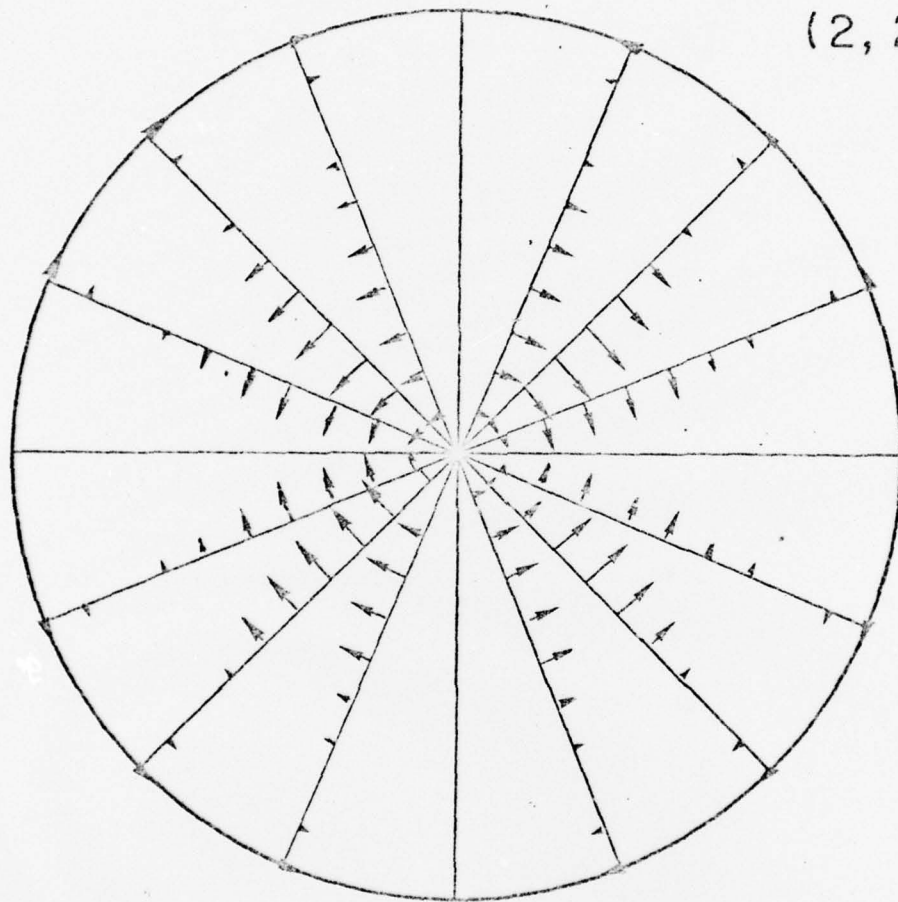
(1, 1)

Fig. 9 (cont'd)

(1,2)

Fig. 9 (cont'd)

Fig. 9 (cont'd)

(2,1)

Fig. 9 (cont'd)

(2, 2)

(a)

Fig. 10

(1,1) 90°

(2,1) 45°   (3,1) 30°

(b)

(1,2) 90°

(2,2) 45°   (3,2) 30°

$u_\theta(r, \theta)$

r/a